6TH Workshop Of
CODE_BRIGHT USERS

13th May 2014
Barcelona, Spain

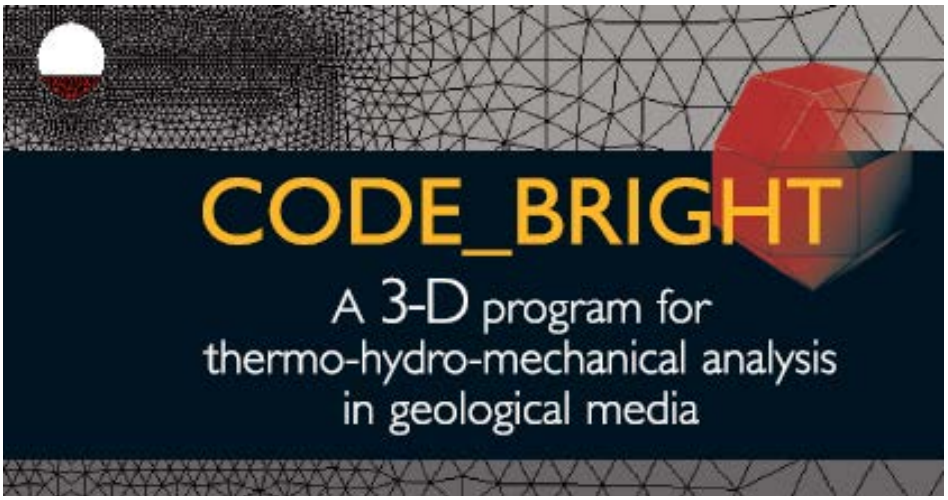

Department of Geotechnical Engineering and Geosciences
(UPC. Barcelona. Spain)
CIMNE
(Centro Internacional de Métodos Numéricos en Ingeniería.
Barcelona. Spain)

CODE_BRIGHT

A 3-D program for thermo-hydro-mechanical analysis in geological media

6th WORKSHOP OF CODE_BRIGHT USERS

Barcelona, 13 May 2014

Department of Geotechnical Engineering and Geosciences

(UPC. Barcelona. Spain)

CIMNE

(Centro Internacional de Métodos Numéricos en Ingeniería. Barcelona. Spain)

CONTENTS

THM Modelling of Final Disposal Repository in Onkalo Project

Erdem Toprak[*], Sebastia Olivella[*], Xavier Pintado †

*Department of Geotechnical Engineering and Geosciences
Technical University of Catalonia (UPC)
Campus Norte UPC, 08034 Barcelona, Spain
Email:erdem.toprak@upc.edu; sebastia.olivella@upc.edu

†B+TECH Oy; Laulukuja 4 00420 Helsinki, Finland
Email:xavier.pintado@btech.fi

Key Words: THM coupled analysis, Friedland Clay, Onkalo Project

Abstract: *This paper describes preliminary results of coupled Thermo-Hydro-Mechanical (THM) processes in the POSIVA ONKALO Project, secondly characterization of Friedland-clay via laboratory tests which will be the backfill material in this project.*

1. INTRODUCTION and PRELIMINARY THM RESULTS

The preliminary analyses of coupled THM processes in ONKALO project have been published by POSIVA OY (POSIVA 2012-47: Thermo-Hydro-Mechanical Modelling of Buffer, Synthesis Report, Toprak et al. 2013). In this report of Posiva, the time required for the buffer to reach full saturation, the maximum temperature reached in buffer, deformations at the buffer-backfill interface and the stress deformation balance in interaction between buffer and backfill also buffer and backfill homogenization were the critical design criteria.

The characteristics of the materials, thermal calculations and preliminary modeling, laboratory test simulations and comparison with measurements and, finally, THM evolution of the deposition hole including a gap have carried out and described in the above mentioned report.

One of the interesting results described in that report is the comparison of temperature evolution for different scenarios (different rock permeability and presence of a gap or not) is presented. When the rock permeability is very low the gap closure is delayed and the temperature increase due to the mentioned isolation effect produced by the gap manages to reach the long term temperature peak. In this case the maximum temperature in the canister is higher by some degrees as compared with the cases where the rock has higher permeability.

Table 1. Evolution of important parameters from THM calculations

Analyzed parameters	Reached values
Maximum temperature in buffer	~ 82 ºC
Time to reach full saturation of buffer	~ 50 years
Achieved maximum suction in buffer	85 MPa
Dry density of buffer	1700-1750 kg/m^3
Swelling pressure of buffer	6-9 MPa
Displacements at the interface of buffer-backfill	10 -16 cm

The most important results that have been obtained in the Posiva Report 2012/47 for buffer material are summarized in the Table 1. These values correspond to the final geometry where buffer disc, buffer ring, backfill, pellet, rock and air-gap are considered as the components of deposition tunnel.

2. MODELLING of FRIEDLAND CLAY via LABORATORY TESTS

At the moment, Friedland clay is considered one of the best candidates to be used as backfill material for the construction of the multiple barrier disposal system for a nuclear spent fuel repository. In order to investigate the hydro-mechanical behavior of Friedland clay, a series of laboratory tests have been started up by B+TECH.

Numerical simulation of two oedometric tests for Friedland Clay has been conducted using Barcelona Basic Model. Figure 1 shows the model performance over test results. The final BBM parameters obtained through the tests for the backfill material are summarized in Table 2. These parameters will be used for long term calculations.

Taking into account updated BBM parameters of Backfill material and including water gap to geometry of the deposition hole and re-performing of THM analyses are upcoming tasks. Modelling of laboratory tests related to homogenization of backfill components, freezing and thawing tests and simulations of gas migration from canister are considered future work for the project of ONKALO.

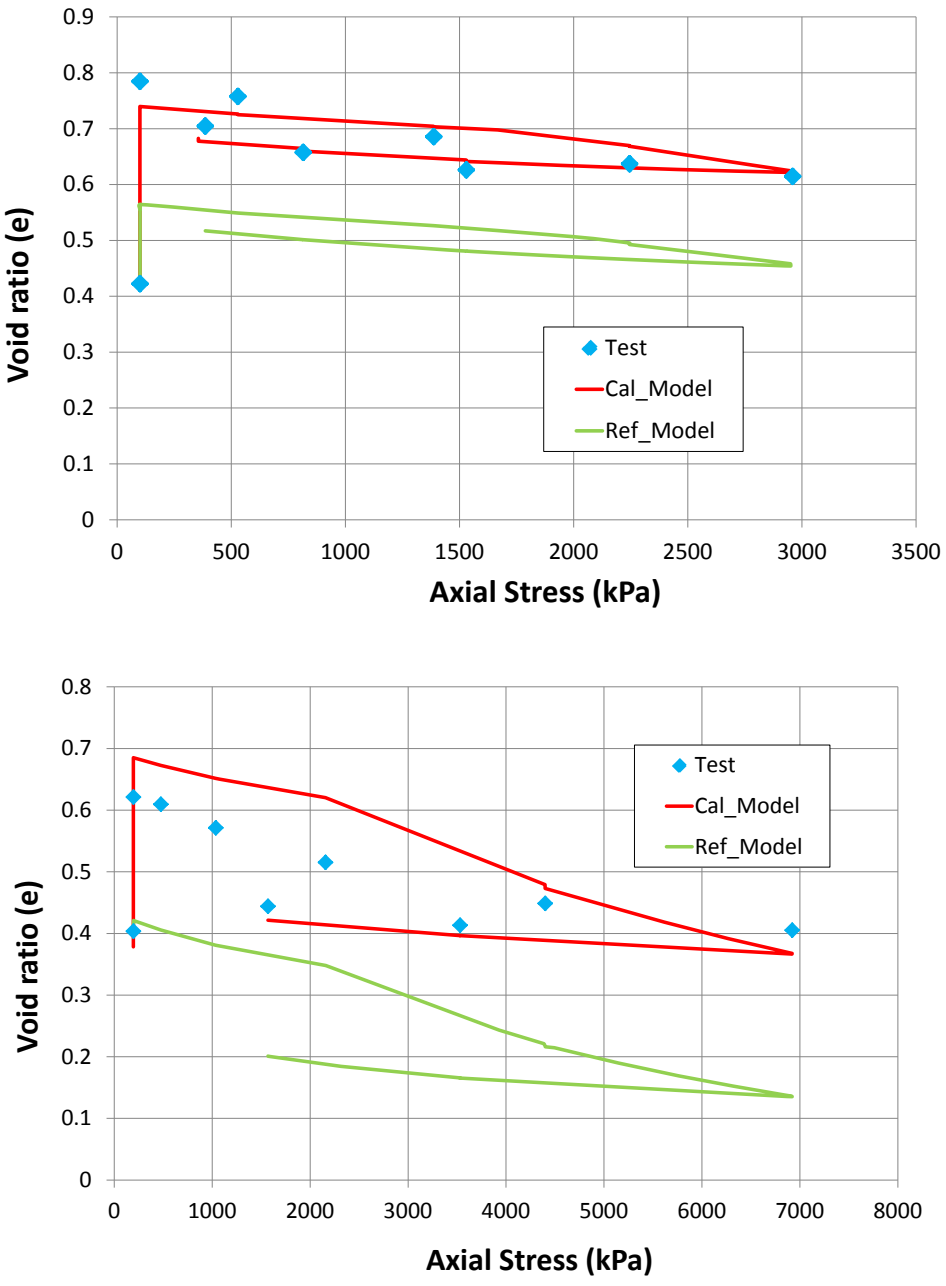

Figure 1. Oedometer tests on Friedland clay. Void ratio versus axial stress

Table 2. BBM parameters for Friedland Clay

Parameters	Symbols	Units	Calibrated
Shear modulus	G	MPa	v=0.25
Parameters for elastic volumetric compressibility against mean stress change	κ_{i0}	-	0.05
	α_i	-	0
Parameters for elastic volumetric compressibility against suction change	κ_{s0}	-	0.05
	α_{sp}	-	0
Slope of void ratio-mean stress curve at zero suction	$\lambda(0)$	-	0.18
Parameters to define LC yield curve	r		0.8
	β	MPa^{-1}	0.02
Reference stress	p^c	MPa	0.1
Initial preconsolidation mean stress for saturated soil	P_o*	MPa	2
Critical state line	M	-	1.07
Intrinsic permeability	k	m^2	$1.6x10^{-20}$
Parameter of water retention curve	P_0	MPa	25
Shape function for retention curve	λ	-	0.38
Power for relative permeability	n	-	3

References

Alonso E.E., Gens A and Josa A, 1990."A constitutive model for partially saturated soils". Géotechnique, 40(3): 405-430

Hokmark. H. 2003. Hydration of the bentonite buffer in a KBS-3 repository. Applied Clay Science 26 (2004) 219 - 233

Ikonen, K. 2003. Thermal Analyses of Spent Nuclear Fuel Repository

Toprak E., N.Mokni, S.Olivella, X. Pintado. (2013) Thermo-Hydro-Mechanical Modelling of Buffer. POSIVA 2012-47.

MODELLING OF DOWN-SCALE TESTS

Pintado X. and Autio J.

B+TECH Oy, Laulukuja 4, FI-00420, Helsinki, Finland
e-mail: xavier.pintado@btech.fi

Key words: Nuclear waste repository, down-scaled tests

Abstract. *The reference nuclear waste repository in Finland is of KBS-3V type. The spent fuel canister is emplaced in deposition holes and embedded in highly compacted bentonite blocks. The gap between blocks and rock is filled with pellets. Down-scaled tests have been carried out in order to study the hydration and swelling process of the blocks and pellets. The modelling of the process has been done with CODE_BRIGHT.*

1 INTRODUCTION

Compacted bentonite is used as a buffer material to make barriers to prevent contamination by isolating the contamination source. High-density compacted bentonite in the form of blocks, discs and rings is used as sealing material in high-level radioactive waste repositories, as it provides very low permeability, sufficient thermal conductivity and adequate mechanical resistance.

The buffer behaviour from emplacement to a saturated state can be simulated with the finite-element code CODE_BRIGHT using relevant constitutive models for buffer and rock. These models require parameters, which are typically determined in small-scale laboratory tests (samples with a 38-100 mm diameter and a 20-150 mm height in [1]). However, in order to reproduce the conditions of the repository more accurately, a number of down-scaled tests have been carried out [2]. For these, some different tests set-ups have been developed. This paper presents the modelling of the Transu test set-up which employs a plastic cell with a diameter of up to 270 mm and a height of 800 mm. The diameter of the blocks is 170 mm, the pellets gap 50 mm and the plastic cell has a thickness of 5.5 mm.

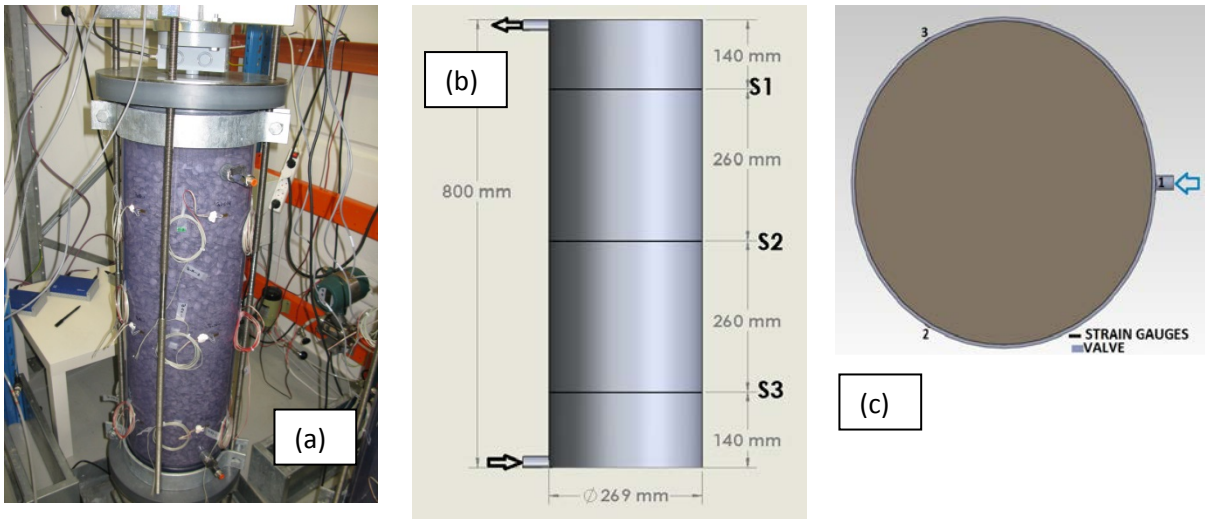

Figure 1. Test set-up (a). Sections of measurement (b) and position of the strain gauges (c). The rows indicates the water inlet and water outlet in (b) and (c)

The axial swelling pressure is measured with a load cell at the top of the sample and the radial strains with strain gauges glued in the plastic cell. In one test, the cell was instrumented with two capacitive hygrometers with wireless data transmission system for measuring the suction evolution of the blocks.

The test simulated in this work is denoted as Transu 8 in reference [2]. This test had constant water pressure at the inlet and the valve of water outlet is closed. The test instrumented with wireless data transmission was Transu 6 in [2]. This test had a constant water flow of 0.1 L/min from the bottom inlet to the top outlet.

The integration of the experimental work and modelling is described in [3].

2 MODEL DESCRIPTION

2.1 Geometry

The geometry has been simulated with one-dimensional mesh. The mesh has 140 nodes and 139 elements: 105 block elements, 28 pellet elements and 6 plastic elements. The calculation is hydro-mechanical (HM), so there are two degrees of freedom per node, liquid pressure and radial displacement.

2.2 Material properties

The mechanical constitutive model chosen has been the viscoplastic model for unsaturated soils based on BBM (Barcelona Basic Model [4]). The elastic parameters are presented in Table 1. The plastic cell has been simulated as isotropic elastic material with E=3145 MPa and n=0.33.

Parameters	Symbols	Units	Blocks	Pellets
Poisson's ratio	υ	-	0.35	0.35
Slope in e - lnp'	a_1	-	-0.002603	-0.1324×10^{-2}
Slope in e – ln((s+0.1)/0.1))	a_2	-	-0.0130	-0.00662
Coupling term	a_3	-	0.1888x10-2	0.96×10^{-3}
Coupling term	a_4	MPa^{-1}	0.7811x10-5	0.3972×10^{-5}
Reference pressure	p_{ref}	MPa	0.01	0.01

Table 1: Elastic parameters of pellets and blocks

The water retention curve chosen has been Van Genuchten model. The values are P_0=65 MPa and λ=0.6 for the blocks and P_0=5 MPa and λ=0.35 for the pellets.

The intrinsic permeability in blocks varies with the porosity following the law $k(\phi) = k(\phi_0) \times e^{(b\times(\phi-\phi_0))}$. The value of $k(\phi_0)$ is 1.12x10^{-19} m^2, b is 15 and ϕ_0 is 0.438 The intrinsic permeability in pellets is kept constant and its value is 10^{-8} m^2. The relative permeability is S_r^3, where S_r is the degree of saturation.

The plastic allows water flow through it. It reproduces the situation of the test when the pellets are an opened structure and the water flows easily through it. When the pellets swell and close the large porous, the conditions of the test changes but the hydraulic conductivity of the pellets is still higher than the block's because of the lower density.

2.3 Initial and boundary conditions

The initial and boundary conditions are described in Table 2.

	Initial condition	Boundary condition
Hydraulic	Blocks: -42 MPa Pellets: -100 MPa PVC: 0.1 MPa	P_l=0.1 MPa
Mechanical	-0.105 MPa	σ_r=-0.105 MPa
Porosity	Blocks: 0.349 Pellets: 0.669 PVC: 0.01	-

Table 2: Initial and boundary conditions

3 SIMULATION RESULTS

The evolution of the axial swelling pressure and radial strains are presented in Figure 2.

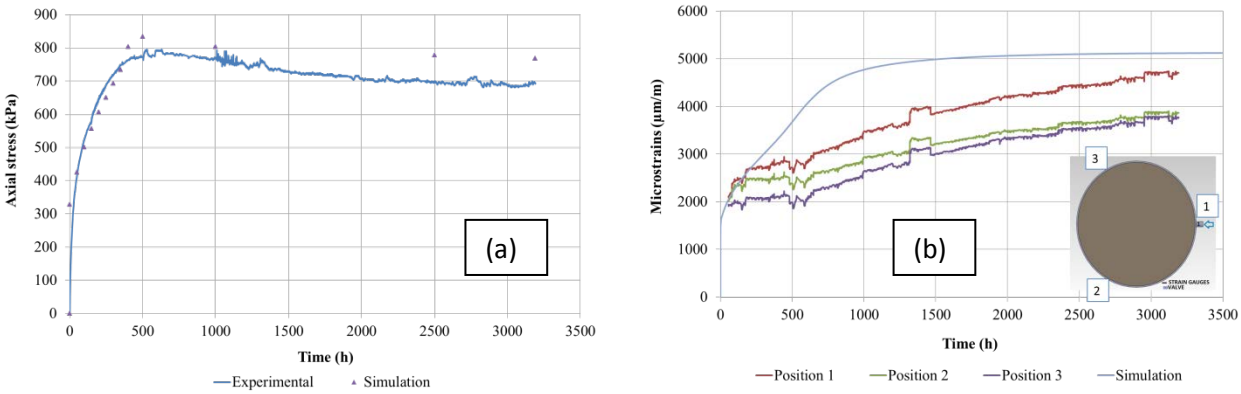

Figure 2: Axial stress evolution (a). Radial strains evolution (b)

The axial swelling pressure presents the average swelling pressure of the system concisiting of pellets filled gap and compacted cylindrical blocks in the center. The evolution can be reproduced quite well although the behavior in maximum shows small differences under the qualitatively point of view.

The radial strains measured and simulated presents also differences under the qualitatively point of view. The initial increase in radial strains is clear but the strains increase more continuously in the experiment than in the simulation. This could be because of the pellets reach the steady state conditions in the simulation relatively fast because of the high intrinsic permeability considered,

which could not be realistic after the pellets swell and the large porous disappear.

The suction evolution was also measured and simulated with CODE_BRIGHT (Figure 3). It is possible to see that although the water inflow is in one point; both measures evolve in a similar way so although the test is clearly three-dimensional, the one-dimensional simulation is able to follow-up quite well the suction evolution.

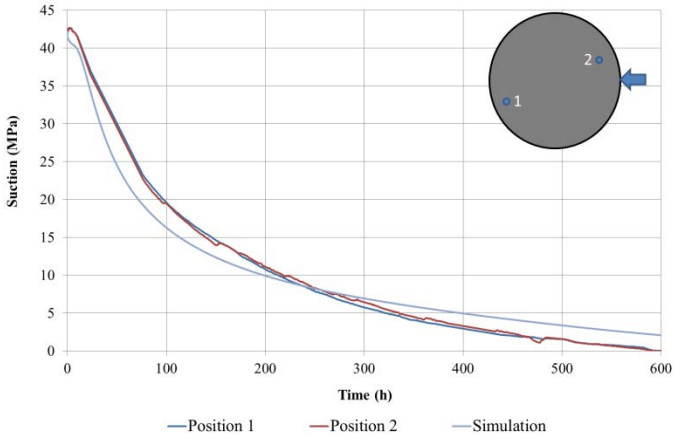

Figure 3. Suction evolution

4 CONCLUSIONS

- The evolution of the axial and radial swelling pressures in a down-scaled test can be simulated although there are some differences under qualitatively point of view.
- The suction evolution is quite well simulated.
- It is possible to use one-dimension meshes for simulating complex 3-D tests taking into account the geometry and process symmetries.

REFERENCES

[1] Pintado, X., Md. Mamunul, H., Martikainen, J. (2013a). Thermo-Hydro-Mechanical Tests of Buffer Material. Posiva report 2012-49. Posiva Oy, Eurajoki, Finland.

[2] Pintado, X., Adesola, F., Turtiainen, M. (2013b). Down-scaled tests on buffer behaviour. Posiva working report 2012-100. Posiva Oy, Eurajoki, Finland.

[3] Pintado, X., Autio, J., Koskinen, K. (2012). Integration of THM-experimental work and modelling to engineered barrier system design. Clay in Natural and Engineered Barriers for Radioactive Waste Confinement. Proceedings of the Meeting “Nantes 2010” – Andra 452 (February 2012): 117-124

[4] Alonso, E.E., A. Gens and A. Josa (1990). A constitutive model for partially saturated soils. Géotechnique, 40(3), 405-430

INTERPRETATIVE MODELLING OF SELECTED IN SITU MEASUREMENTS OBTAINED AT URL MONT TERRI USING CODE_BRIGHT

O. Czaikowski, M. Komischke & K. Wieczorek

Gesellschaft für Anlagen und Reaktorsicherheit (GRS) mbH
Theodor-Heuss-Strasse 4, 38122 Braunschweig, Germany
e-mail: oliver.czaikowski@grs.de, web page: http://www.grs.de

Key words: in situ measurements, HM coupled analysis, DM-B, URL Mont Terri

Abstract. *Regarding the tight coupling between fluid flow processes and mechanical deformation in argillaceous rock mass this paper presents selected experimental findings obtained in the URL Mont Terri which are interpreted by physical modelling and numerical simulation using CODE_BRIGHT. Within the interpretative modelling process, 2D numerical modelling work, reflecting the actual properties of the rock in situ, is performed and the simulation results are compared to the experimental findings.*

1 INTRODUCTION

The international experience gained in the field of geological radioactive waste disposal indicates that coupling between thermal, hydraulic, mechanical and chemical processes (THMC-coupling) in claystone rock mass will be much more significant than in salt rock formations. The fabric components, saturation level and pore water pressure determine the load bearing behavior of the claystone rock mass affected by the impact of excavation activity and waste storage related aspects.

It is widely agreed that the overall detection of geohydraulic conditions and their changes due to geomechanical disturbances via in situ measurements is one of the most relevant prerequisites for reliable physical modelling and numerical simulation of coupling processes. With respect to disposal in argillaceous formations, GRS therefore performs experiments at URL Mont Terri. Figure 1 shows a sketch overview of selected GRS in situ measurements within the experiments DM-A/B[i] and HE-E[ii] at URL Mont Terri.

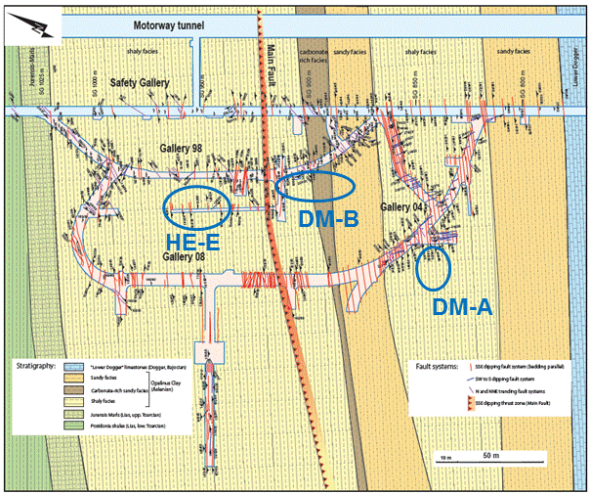

Figure 1: Overview of selected in situ measurements at URL Mont Terri in which GRS is involved

2 PHYSICAL MODELLING AND NUMERICAL SIMULATION

For reliable physical modelling and numerical simulation the applied constitutive model must be able to represent the test itself (e.g. increase in pore and/or packer pressure for permeability tests) as well as the corresponding behaviour of the surrounding rock mass as a consequence of the initial boundary conditions (e.g. slightly decrease of pore and/or packer pressure down to initial values after the test procedure). Within the interpretation process, 2D numerical modelling work, reflecting the actual properties of the rock in situ, is performed and the simulation results are compared to the experimental findings.

2.1 Physical modelling

In the framework of the presented modelling exercise the computer code CODE_BRIGHT developed by UPC is used for 2D analysis of coupled thermo-hydro-mechanical (THM) phenomena in geological media. The idea of GRS' simulations is to use simple standard models installed in CODE_BRIGHT to try to model the rock behaviour in the DM-B experiment. The theoretical framework is formed of three main parts: balance equations, equilibrium restrictions and constitutive equations. Balance equations are solved for solid, liquid, and gas phases, as well as for energy and momentum. The liquid phase may contain water and dissolved air, and the gas phase may be a mixture of dry air and water vapour. Thermal equilibrium between phases is assumed. Equilibrium restrictions are given for the concentration of water vapour in gas via the psychrometric law and for the concentration of dissolved air in water via Henry's law. Details about the basic theories with the formulated governing equations are described in the code manual[iii].

The constitutive equations establish the link between the independent variables and the dependent variables. They are assigned to the material parameters compiled in Table 1, which are published in a recent report[iv].

Parameter	Unit	Symbol	OPA
(a) Physical parameters			
Solid grain density	kg/m^3	ρ_S	2700
Initial porosity	-	ϕ_0	0.137
(b) Hydraulic parameters			
Anisotropic permeability	m^2	$K_{//}$ $K_{\perp}$	2.0E-19 5.0E-20
Liquid rel. permeability	-	λ	3
Liquid rel. permeability	-	A	1
Vapour diffusion coefficient	m^2/s	D	5.9E-06
Tortuosity	-	τ	1
Exponent	-	n	2.3
Retention curve	MPa	P_0	12
Retention curve	N/m	σ_0	0.072
Retention curve	-	γ	0.3
Retention curve	-	S_{rl}-S_{rs}	0.01-1.0
(c) Mechanical parameters			
Young`s modulus	MPa	E	3000
Poisson ratio	-	ν	0.29
Viscosity	MPa·s	η	2.1E-12
(d) Coupling parameters			
Biot coefficient	-	b	1.0

Table 1: Material parameters determined for Opalinus Clay

For the hydraulic problem it is assumed that the liquid and gas flows follow Darcy's law, with the actual effective permeability to each phase being given by the product of intrinsic and relative permeability. The dependence of intrinsic permeability k on porosity ϕ is given by

$$k = \mathbf{k}_0 \cdot \frac{\phi^3}{(1-\phi)^2} \cdot \frac{(1-\phi_0)^2}{\phi_0^3}$$

with initial values k_0 and ϕ_0. The relative permeabilities of the liquid and gaseous phases are dependent on the degree of liquid saturation according to

$$S_e = \frac{S_l - S_{lr}}{S_{ls} - S_{lr}} \quad \text{and} \quad k_{rl} = A \cdot S_e^{\lambda} \quad k_{rg} = 1 - k_{rl},$$

where S_l, S_{lr}, S_{ls}, S_e are the actual, residual, maximum and effective saturation of liquid, respectively, and A and λ are parameters. It is necessary to define the retention curve of the materials relating the degree of saturation to suction. Generally, the formulation of van Genuchten with material parameters β, P_0 and σ_0 is selected.

$$S_e = \left[1 + \left(\frac{P_g - P_l}{P}\right)^{1/(1-\beta)}\right]^{-\beta} \quad \text{where} \quad P_g - P_l \geq 0 \quad \text{and} \quad P = P_0 \cdot \frac{\sigma}{\sigma_0}$$

The molecular diffusion of vapour is governed by Fick's law, a constant dispersion coefficient corresponding to the molecular diffusion of vapour in air is assumed.

$$D_m^w = \tau D \left(\frac{(273.15 + T)^n}{P_g}\right)$$

where P_g is given in MPa. For the tortuosity τ a value of 1.0, for n a value of 2.3 and for D a value of 5.9E-6 m²/s were adopted.

Regarding mechanical behaviour, all materials were modelled as poroelastic. Damage was not considered. Time-dependent deformation is only possible as a consequence of pore pressure variation.

The geometrical model is a plane-strain vertical section through the borehole BDM-B1 and the Gallery 98 with horizontal bedding plane orientation. Figure 2 shows the model together with the mechanical boundary conditions.

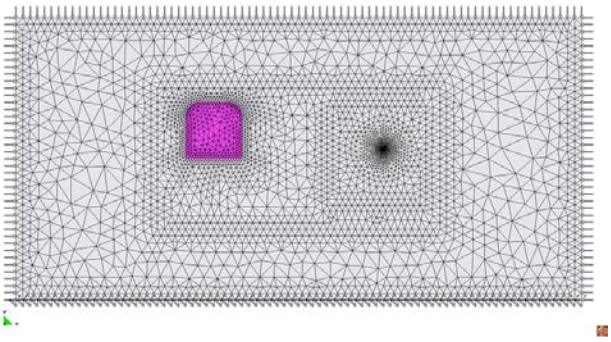

Figure 2: 2D model used for modelling of pore pressure evolution in boreholes BDM-B5/6/7/8

The initial state is given by a rock temperature of 14 °C, an isotropic stress state of 4.0 MPa, and an assumed primary pore pressure of 2 MPa. The pore pressure distribution, however, was significantly disturbed by the ventilation of the Gallery 98 from 1998 up to

2013. Therefore, the history of the test region had to be taken into account. This was down in a simplified way, by fixing a high suction value of -5 MPa on the Gallery wall to simulate the ventilation. With installation of the BDM-B1, the suction on the contour is set to -2 MPa according to a relative humidity value of 98%. Ten days after installation atmospheric pressure was fixed on the borehole contour.

2.2 Experimental findings compared to simulation results

Figure 3 shows the test location at the Gallery 98 and the corresponding 2D model. The test layout was designed to have some of the pore pressure sensors in the immediate vicinity of the borehole BDM-B1 to be able to measure the reaction of the pore pressure in the borehole nearfield as a consequence of the excavation process, while the two sensors in BDM-B7+8 should be able to identify changes in pore pressure evolution due to the boundary of the sandy and carbonate rich facies.

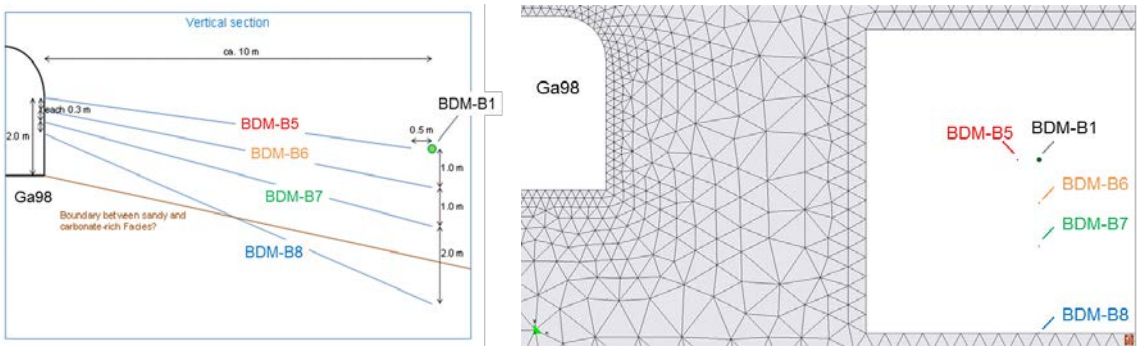

Figure 3: Test layout at Gallery98 and corresponding 2D model

Figure 4 (left) gives an impression of pore pressure measurements in the boreholes BDM-B5/6/7/8. While sensor BDM-B8 shows a constant pore pressure value around 6 to 7 bars, the sensor BDM-B5 shows a value slightly above atmospheric pressure, that might be related to the short distance to the excavated borehole. The sensor in borehole BDM-B6, which is also in the direct vicinity of BDM-B1 shows a certain drop in pressure after the excavation process that could be related to the drainage effect and the partial unloading of the borehole EDZ.

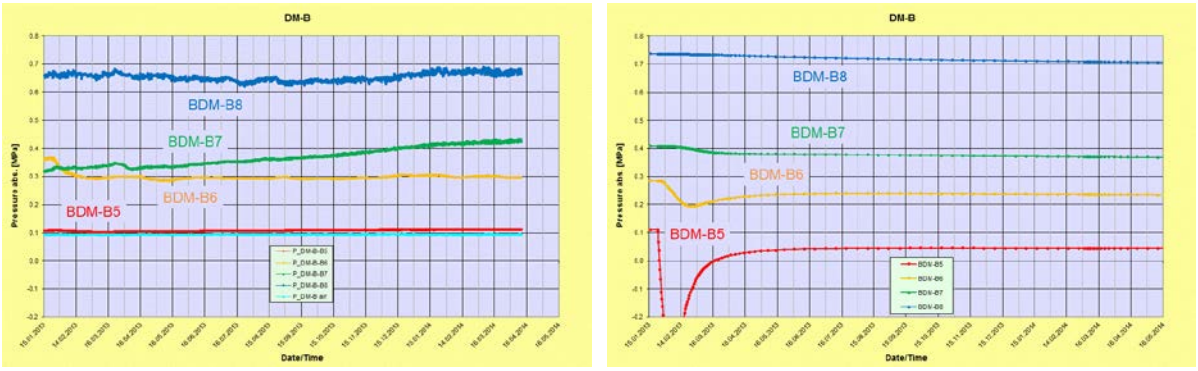

Figure 4: Experimental findings of fluid pressure measurements in boreholes BDM-B5/6/7/8 (left) compared to numerical results for pore pressure values (right)

Regarding the long-term behavior of BDM-B6 the pore pressure stabilizes at a value of 3 bar, whereas sensor BDM-B7 shows more or less a stationary increase in pore pressure during the following 15 month.

With respect to the experimental findings the numerical results show generally an adequate agreement within the considered borehole measurements, especially the level of pore pressure in all sensors before borehole excavation in January 2013. The evolution of the calculated pore pressure with time at BDM-B6 is nearly identical to the measured ones.

In contrast to the measurement at BDM-B7, a pore pressure decrease can be observed in the simulation (Figure 4 right). At BDM-B5 close to the excavated borehole, even negative pore pressure (suction) is calculated. Suction cannot be detected by the installed measuring transducers. Therefore Figure 4 (left) shows pore pressure values near to atmospheric pressure. The measured slight increase in pore pressure with time of about one tenth of a bar could, on the other hand, be interpreted as the start of a recovery process of the pore pressure field that might take more time than 15 month.

The results for BDM-B7 and BDM-B8 post excavation for the evolution of pore pressure with time agree less well. Modelling still needs refinement, this is currently in process.

3 CONCLUSIONS

The simplified approach is in principle able to describe the tight coupling between fluid flow processes and mechanical deformation in argillaceous rock mass. Regarding the modelling results for the pore pressure sensors that agree less well to the experimental findings the applied constitutive model may need to be improved with regard to adequate modelling of damage and self-sealing processes and induced permeability changes. Further work will be done within the framework of the EC project DOPAS, jointly funded by Euratom's Seventh Framework Programme and the German national funding organization BMWi.

4 ACKNOWLEDGEMENTS

The authors gratefully acknowledge the funding by the German Ministry of Economics and Energy (BMWi) under contract no. 02 E 10377 and 02 E 10689. We would also like to thank our colleagues from the Mont Terri Project and from the Technical University of Clausthal for support and the fruitful cooperation during the execution of the experiments.

REFERENCES

[i] DM-B Experiment: Long-term deformation measurements (Extension of DM-A Experiment). 5-Pager, Mont Terri Project, Experimental Programmes, 30th April 2012.

[ii] HE-H Experiment: In-situ Heater Experiment on Key THM Processes and Parameters. 5-Pager, Mont Terri Project, Experimental Programmes, 30th April 2012.

[iii] CODE_BRIGHT, 2002. A 3D program for thermo-hydro-mechanical analysis in geological media. Users guide

[iv] HE-E Experiment: Lay-out, Interpretation and THM Modelling. Garrite, B.; Gaus, I. (Eds.). Wieczorek, K.; Czaikowski, O.; Senger, R.; Gens, A.; Vasconcelos, R.; Schuster, K.; Mayor, J.C.; Garcia-Sineriz, T.; Trick, T. Combining D2.2-11: Final report on the HE-E experiment and D3.2-2: Modelling and interpretation of the HE-E experiment of the PEBS Project), in preparation.

THE EFFECT OF GEOMETRICAL DISPOSITION OF IMPERMEABLE MEMBRANES ON THE SUBGRADE SERVICE LIFE OF RAIL TRACK EMBANKMENTS

Matteo O. Ciantia*, Joaquín Pérez-Romero†, Jean Vaunat* and Marcos Arroyo*

* Department of Geotechnical Engineering and Geosciences (ETCG)
Universidad Politécnica de Cataluña
Campus Norte UPC, 08034 Barcelona, Spain
e-mail: ciantia.matteo@gmail.com, www.etcg.upc.edu

† Escuela de Arquitectura
Grupo de Investigación HUM-064
Universidad de Malaga
Plaza el Ejido s/n. Campus El Ejido. 29071. Málaga, Spain
e.mail: joaquin.perez@uma, www.arquitectura.uma.es

Key Words: *Railroad engineering; Embankment design; Unsaturated soils; Environmental loads*

This paper discusses the effect of the geometrical disposition of impermeable membranes in the overall performance of railway embankments on the basis of a methodology suitable to account for the effects of rail traffic loading and environmental actions over its service life. To emphasize the effect of the water impermeable layers on the atmospheric induced embankment irreversible deformations, both dry and wet climate conditions were investigated. AASHTO indications were used to account for such weather induced permanent deformations and hence the mechanical design of the railway track is first analyzed through a two-dimensional finite-element (FE) mode. Then, a two-dimensional FE hydro-thermic analysis is developed to assess the effect of the different solutions in the performance of the embankment resulting from environmental effects (atmospheric actions and position of the phreatic level). Results from the mechanistic and hydro-thermic analysis were combined to predict the long-term deformational behavior of the subgrade. The numerical results show how the position of the impermeable membrane affects the service life of the embankment.

1 INTRODUCTION

The present paper focuses on the use of impermeable membranes layers in railway trackbed design and on their potential to protect the substructure over its service life. It describes a suitable methodology to account for the effects of traffic loading and environmental actions in the hydro-thermo-mechanical performance of the subgrade and consequent deformational behavior over time. Thus, the effect of the use and the geometrical disposition of impermeable membranes in the overall performance of railway embankments is assessed. The methodology is based on a mechanistic-empirical design approach [i]. The Railway track mechanical problem is solved first using an uncoupled finite-element (FE) model giving the embankment deformation induced by a single purely mechanical loading cycle. Subsequently a hydro-thermic analysis using the concepts of continuous mechanics is performed in order to evaluate, according to the environmental climatic conditions, the hydro-thermal response of the embankment. Finally, an empirical approach similar to mechanical-fatigue calculations is applied to estimate the coupled long term mechanical-atmospheric induced deformations. The paper is hence divided into two sections: i) Hydro-thermal (T-H) analysis of the railway track, accounting for environmental variables such as hydro-geological conditions (phreatic level) and atmospheric actions (precipitation, temperature, and relative

humidity) when modeling the runoff of superficial rainwater; and ii) results from the mechanical and hydro-thermal analysis are combined to predict the long-term deformational behavior of the subgrade for the different considered subballast solutions.

2 MODELING ENVIRONMENTAL ACTIONS ON RAILWAY TRACK

The aim of the analysis developed in the present paper is to assess the effect of the geometrical disposition of impermeable membranes in the overall performance of railway embankments on the basis of a methodology suitable to account for the effects of rail traffic loading and environmental actions over its service life. The geometrical specifications together with the type of weather and boundary conditions imposed are listed in Table 1. The CODE_BRIGHT FE numerical tool [ii] is used to perform all the TH analyses described subsequently.

Table 1 Test ID, climate and geometrical disposition of impermeable membranes

Test ID	DRY-1	DRY-2	WET-1	WET-2
Icon	NU_B, 10 m, 2 m	NU_B, 10 m, 2 m	NU_B, 10 m, 2 m	NU_B, 10 m, 2 m
Climate				

2.1 CODE_BRIGHT 2D T-H Model

Atmospheric boundary condition options in CODE_BRIGHT allow imposing boundary conditions in terms of evaporation, rainfall, radiation and heat exchanges thus simulating soil-atmosphere interactions.

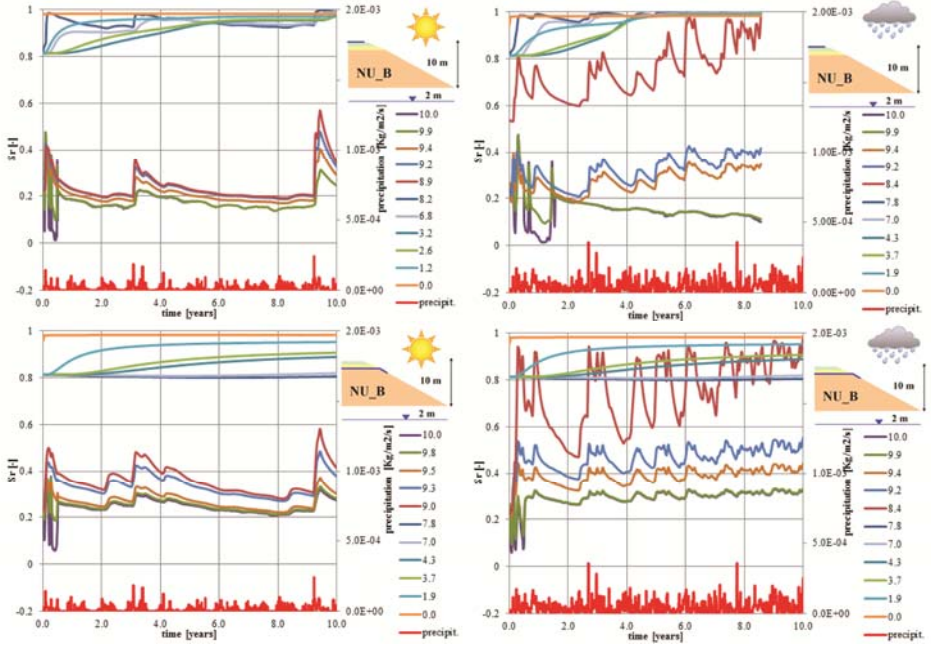

Figure 1: Effect of geo-membrane disposition on saturation degree evolution in dry (left) and wet (right) climate.

These phenomena are expressed as flux boundary conditions for the three components (water, air and energy) as functions of the state variables (liquid pressure, gas pressure and

temperature of the soil) or dependent variables (liquid saturation degree, fraction of water in the gas phase) and meteorological data that vary in time (atmospheric temperature and pressure, relative humidity, solar radiation, cloud index, rainfall and wind velocity). In this work atmospheric boundary conditions taken from a dry (Antequera) and wet (San Sebastián) climate are considered. The simulation considers 10 years of atmospheric action on a 10 m well compacted embankment. The results of the four conditions here discussed are represented in Figure 1.

3 LONG TERM DEFORMATION BEHAVIOR

The overall permanent deformation for a given season is the sum of permanent deformation for each individual layer and is mathematically expressed as:

$$RD = \sum_{i=1}^{nsublayers} \varepsilon_p^i h^i \tag{1}$$

Where RD is the pavement deformation, ε_p^i is the total plaic strain of the sublayer *i*, and h^i is is the thinkness of the sublayer. The permanent deformation in unbound materials is calculated following the basic relationship proposed by Tseng and Lytton [iii]

$$\delta_a(N) = \beta_1 \left(\frac{\varepsilon_0}{\varepsilon_r} \right) e^{-\left(\frac{\rho}{N}\right)^\beta} \varepsilon_v h \tag{2}$$

Where δ_a is the layers' settlement; N is the number of traffic repetitions; $\varepsilon_0, \beta, \text{and } \rho$ are fatigue coefficients of the material; ε_r is the strain imposed in the laboratory to calculate $\varepsilon_0, \beta, \text{and } \rho$; ε_v is the vertical deformation obtained with the pseudo elastic mechanical model; h is the thickness of the layer and β_1 is a calibration factor. The fatigue coefficients that appear in the model were recalibrated for thei application [i]. The results can be expressed as:

$$\log \beta = -0.61119 - 0.017638 W_c \tag{3}$$

$$\log\left(\frac{\varepsilon_0}{\varepsilon_r} \right) = 0.5 \left[e^{(\rho)^\beta} a_1 + e^{\left(\rho/10^9\right)^\beta} a_9 \right] \tag{4}$$

$$C_0 = \ln\left(\frac{a_1}{a_9} \right) \tag{5}$$

$$\rho = 10^9 \left(\frac{C_0}{\left(1 - \left(10^9\right)^\beta\right)} \right)^{\frac{1}{\beta}} \tag{6}$$

Where W_c is the water content (%), and a_1=0.15 and a_9=20. AASHTO proposes an empirical expression for the water content as a function of the water table depth and the reference resilient modulus. In this work, following [iv][v] the water content is taken from the T-H analyses performed with CODE_BRIGHT presented above. Finally the calibration factor is equal to 1.673 for unbound granular bases while it is equal to 1.35 for all subgrade soils. To determine ε_v a mechanical analysis is performed and the results are represented in Figure 2. Finally, using eqs. (1)-(6), the irreversible weather induced deformations, employing the T-H results previously presented, are computed and reported in Figure 3.

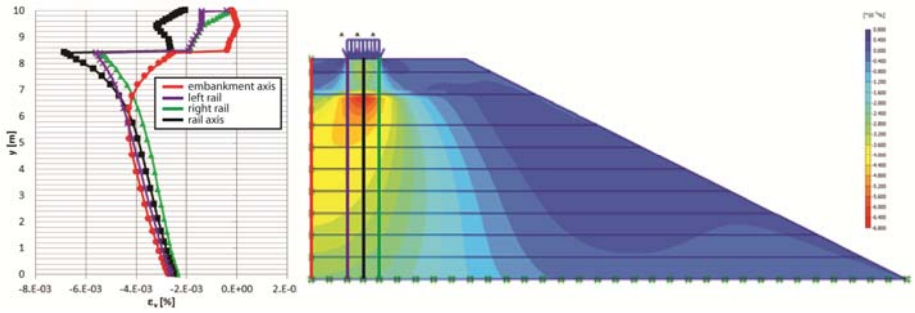

Figure 2: Embankment vertical deformation due to equivalent static load.

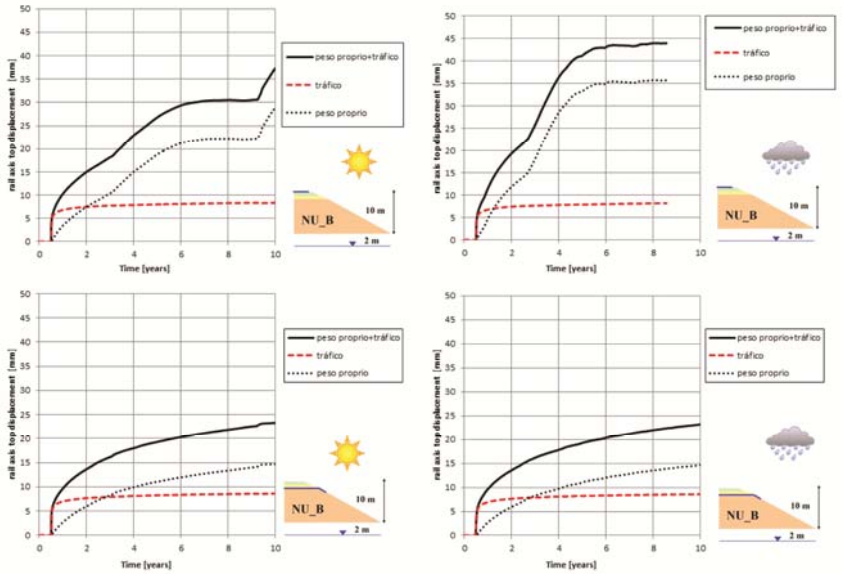

Figure 3: Effect of geo-membrane disposition on saturation degree evolution in dry (left) and wet (right) climate.

4 CONCLUSIONS

The long-term deformational behavior of the railway trackbed was predicted considering the effects of water content variations and traffic loading over time. The proposed solutions that incorporated impermeable membrane between the granular base and the clayey nucleus showed a better performance than the ones without interlayer impermeable membrane concerning the substructure's predicted service life. This work was realized within the FASTRACK project, supported by CDTI and FEDER European Union founds.

REFERENCES

[i] AASHTO. (1993). Guide for the design of pavement structures, Washington, DC.

[ii] Olivella, S., Gens, A., and Alonso, E. E. (1996). "Numerical formulation for a simulator (CODE_BRIGHT) for the coupled analysis of saline media." Eng. Comput., 13(7), 87–112.

[iii] Tseng, K. H., and Lytton, R. L. (1989). "Prediction of permanent deformation in flexible pavement materials." Implication of aggregates in the design, construction, and performance of flexible pavements, ASTM, Philadelphia, 154–172.

[iv] Ferreira, T. M., Teixeira, P. F., and Cardoso, R. (2011). "Impact of bituminous subballast on railroad track deformation considering atmospheric actions." J. Geotech. Geoenviron. Eng., 137(3), 288–292.

[v] Ferreira, T. M., & Teixeira, P. F. (2012). Rail Track Performance with Different Subballast Solutions: Traffic and Environmental Effects on Subgrade Service Life. J. of T. Eng, 138(12), 1541-1550.

FIRST-TIME FAILURE MECHANISMS INDUCED BY SLOPE-VEGETATION-ATMOSPHERE INTERACTION: THE CASE STUDY OF A FISSURED CLAY SLOPE

Giuseppe Pedone[*], Aikaterini Tsiampousi[†], Federica Cotecchia[*] and Lidija Zdravkovic[†]

[*] Department of Civil, Environmental, Territorial, Construction Engineering and Chemistry
Technical University of Bari
Via Orabona 4, 70125 Bari, Italy
e-mail: giuseppe.pedone@poliba.it, federica.cotecchia@poliba.it

[†] Department of Civil and Environmental Engineering
Imperial College London
Skempton Building, London SW7 2AZ, UK
e-mail: aikaterini.tsiampousi05@imperial.ac.uk, l.zdravkovic@imperial.ac.uk

Key words: fissured clay, unsaturated soil, landslide, finite element, ICFEP, first-time failure

Abstract. *This paper presents the case study of the Pisciolo hill-slope, which is representative of deep and slow landslide processes in clay slopes that recurrently affect the Southern Apennine. According to monitoring data interpretations and limit equilibrium analyses, rainfall infiltration constitutes the main factor triggering such instabilities. In order to clarify the connection between slope movements and climatic effects, a finite element simulation was conducted with reference to the Pisciolo case study, whose results are here briefly summarized.*

1 INTRODUCTION

Deep (more than 30 m) and slow (1-20 cm/year) instabilities are recurrently observed in heterogeneous and tectonized clay slopes in the Southern Apennine. Landslide accelerations are generally observed at the end of winter, when the highest piezometric heads are registered at depth due to rainfall infiltration. Consequently, the latter represents the main triggering factor for instabilities, while the main predisposing factor is represented by the fissuring of the clay materials forming the unstable slopes. Fissured clays are characterized by higher permeabilities and lower strengths with respect to the same material when reconstituted. In this paper the Pisciolo case study[i] is reported, which is representative of the above mentioned processes. The particular site was chosen because the landslide movements produced severe damages to important infrastructures.

2 THE PISCIOLO CASE STUDY

Three main soil units have been identified on the Piscilo hill-slope after conducting several surveys and analyzing the borehole corings[i]. The deepest one, part of the Red Flysch formation, is mainly constituted of fissured clays including calcarenitic blocks. This unit outcrops in the central portion of the unstable area, while sandstones and sands outcrop in its margins, where the Numidian Flysch formation has been identified. An intermediate unit

outcrops on the rest of the hill-slope. It is mainly formed of active (A=0.85) fissured clays (CF=40-60%) interbedding fractured rock blocks.

Based on stereoscopic analysis of aerial photos and monitoring data interpretation[i], the geo-morphological setting of the hill-slope has been identified. It is characterised by the presence of roto-translational landslides, from slow to extremely slow, whose shear band positions are from intermediate to deep. All the instabilities essentially involve the fissured clay of the intermediate unit, which is characterized by low mechanical strength (up to φ'=18.5° and c'=20 kPa above 25 m depth). The latter further decreases with depth (up to φ'=14.5° and c'=8.5 kPa below 25 m depth), promoting the formation of deep shear bands[i].

Laboratory measurements of permeability on intact samples roughly range between 10^{-10} and 10^{-11} m/s, while in situ measurements are higher than 10^{-9} m/s. Reconstituted clays of similar composition are characterised by permeabilities even lower than those measured in the laboratory, demonstrating that fissuring increases the hydraulic conductivity of the intact material, assisting rainfall infiltration[ii]. The fissured meso-structure also affects the unsaturated soil behaviour, as observed by testing the Pisciolo fissured clay both with the filter paper technique and the Imperial College high capacity tensiometers[ii].

The landslide bodies were monitored by means of both inclinometers and GPS sensors, that registered the maximum velocities (up to 18 cm/year) at the end of winter, in conjunction with the maximum hydraulic heads. The latter were measured at the same depths as the shear bands (up to 50 m) using both electrical and Casagrande piezometers. Also the 6-month cumulative rainfall presents its maximum values at the end of winter, thus supporting the hypothesis that rainfall infiltration represents the main factor triggering the instabilities. In fact, infiltration of rain water at depth induce pore pressure increase, shear strength reduction and consequent landslide acceleration[i].

The phenomenological interpretation of the landslide mechanism has been corroborated by performing limit equilibrium analyses with reference to the most active landslide bodies. The pore pressure distribution employed in such analyses has been obtained by means of finite element simulations aimed at reproducing the slope-vegetation-atmosphere interaction[ii]. Such simulations highlighted the strong influence that both permeability heterogeneities and evapo-transpiration processes have on the piezometric regime of the hill-slope. The latter is characterized by seasonal fluctuations of the pore pressures (0.5-4 m) even at great depths.

3 NUMERICAL MODELLING

In order to investigate in detail the effect of slope-vegetation-atmosphere interaction on landslide stability, fully coupled hydro-mechanical simulations were performed with the finite element code ICFEP[iii]. A constitutive model[iv] similar to the Barcelona Basic Model[v] was used in the simulations, because the soil interacting with the vegetation and the atmosphere is generally partially saturated. The yield and plastic potential functions implemented in the model correspond to those proposed by Lagioia et al., conveniently modified by Tsiampousi et al.[iv] with reference to the dry side, in order to avoid shear strength overestimations. According to the framework proposed by Alonso et al.[v], expansions of the elastic region occur when suction increases. In fact, an apparent cohesion proportional to the suction value is integrated in the model, as well as the variation of the isotropic yield stress due to suction changes (that defines the loading collapse curve[v]). Also a suction increase yield surface is

included in the constitutive model, together with an expression that links the elastic compressibility of the material to its degree of saturation[vi].

Before analyzing the boundary value problem, oedometer and triaxial tests were numerically simulated[ii] in order to calibrate the saturated behaviour of the Pisciolo fissured clays. Unconfined drying tests were also simulated[ii], combining the constitutive model with the water retention function proposed by van Genuchten and with a hydraulic conductivity function matching the one proposed by the same author. Unconfined drying tests, however, are not sufficient for a full calibration of the unsaturated soil behaviour, so the loading collapse curve was assumed to be linear. This is a reasonable assumption for the analysed case study, in which the unsaturated soils are all located at shallow depths, thus being subjected to very low total stresses. Moreover, all the suction induced deformations were assumed to be elastic, but the change in compressibility with suction was carefully calibrated[ii], in particular relating the elastic compressibility to the degree of saturation.

Numerical modelling[ii] was conducted with reference to a section representative of the most active portion of the Pisciolo hill-slope, characterized by an inclination slightly higher than 12°. Such a profile resulted from an excavation conducted at the toe of the slope and along it, with the aim of simulating the erosion produced by both the river and the runoff processes. K_o=1 was assumed before the excavation, as suggested by the geo-structural history of the hill-slope that altered the stress distribution subsequent to the material deposition. The lateral boundaries of the model (Fig. 1) were considered horizontally constrained during the entire simulation, while the bottom boundary was considered fully fixed. As for the hydraulic boundary conditions, both lateral and bottom boundaries were assumed impervious, while on the top boundary a constant suction of 40 kPa was applied during the excavation.

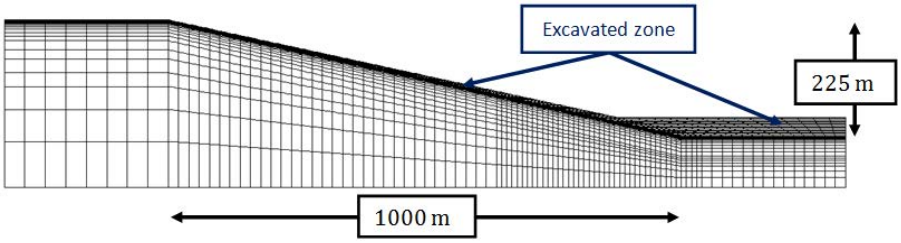

Figure 1: Mesh generated for the slope stability analysis of the Pisciolo case study.

Aim of the excavation phase was the definition of a model that was hydro-mechanically representative of the real slope, i.e. also characterised by void ratio and permeability variations with depth similar to the ones measured. After the initialisation phase, a consolidation analysis was performed, in which daily net rainfalls were applied on the top boundary of the mesh. Net rainfalls were calculated as the difference between gross rainfalls and evapo-transpiration fluxes, the latter estimated by means of the FAO Penman-Monteith method on the basis of temperature measurements. Run off processes were also indirectly taken into account by employing a precipitation boundary condition that is able to prevent rainfall infiltration once the pore pressures are close to 0 kPa on the top boundary of the mesh.

The piezometric regime of the hill-slope was well reproduced by the numerical model, with the seasonal pore pressure variations being close to those measured in situ, especially with reference to intermediate depths. It is also worth noting that, consistent with the pore

pressure fluctuations, a shear band propagates within the slope, starting from the toe and defining the geometry of a potential landslide body of intermediate depth (Fig. 2). Consequently, first-time failure mechanisms are likely to form due to the slope-vegetation-atmosphere interaction, the latter representing the main factor causing the formation of landslide bodies in the clay slopes located along the Southern Apennine.

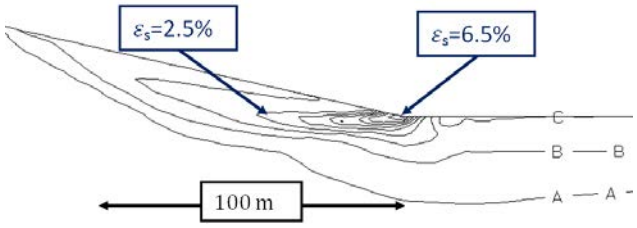

Figure 2: Contours of plastic shear strains accumulated after few years of net rainfall.

4 CONCLUSIONS

- The paper reports the results of a fully coupled hydro-mechanical analysis with reference to a rainfall-induced landslide in a clay slope, where the slope-atmosphere-vegetation interaction was accurately simulated.
- The results suggest that first-time failure mechanisms can be triggered by pore pressure fluctuations occurring due to combination of infiltration and evapo-transpiration processes.
- Further analyses will account for the fractured rock blocks, frequently identified within the hill-slope. Due to these heterogeneities, large pore pressure fluctuations are caused at great depths, possibly inducing the formation of a deeper shear band.

REFERENCES

[i] F. Cotecchia, G. Pedone, O. Bottiglieri, F. Santaloia, C. Vitone, 2014, "Slope-atmosphere interaction in a tectonized clayey slope: a case study", Italian Geotechnical Journal, Vol 1/14, pp. 32-59.

[ii] G. Pedone, 2014, "Interpretation of slow and deep landslides triggered by slope-atmosphere interaction in slopes formed of fissured clayey turbidites", PhD thesis, Technical University of Bari, Italy.

[iii] D. M. Potts, L. Zdravkovic, 1999, "Finite element analysis in geotechnical engineering: Theory", Thomas Telford, London.

[iv] A. Tsiampousi, L. Zdravkovic, D. M.Potts, 2013, "A new Hvorslev surface for critical state type unsaturated and saturated constitutive models", Computers and Geotechnics, Vol 48, No 2, pp. 156-166.

[v] E. E. Alonso, A. Gens, A. Josa, 1990, "A constitutive model for partially saturated soils", Géotechnique, Vol 40, No 3, pp. 405-430.

[vi] A. Tsiampousi, L. Zdravkovic, D. M.Potts, 2013, "A three-dimensional hysteretic soil-water retention curve", Géotechnique, Vol 63, No 2, pp. 155-164.

MODELLING COLLAPSE AND FAILURE OF VOLCANIC SLOPES UNDER CLIMATIC ACTIONS

Villarraga C., Ruiz D., Vaunat J, and Casini F.

Department of Geotechnical Engineering and Geosciences, UPC, Barcelona, Spain

Key words: Rainfall, landslides, pyroclastic materials, CODE-BRIGHT

Abstract. *Landslides induced by rainfall represent a significant natural hazard for large part of Europe. The catastrophic flowslides that occurred on steep slopes in Campania (southern Italy) in 1998, 1999, and 2005 were triggered by rainwater infiltration into shallow deposits of pyroclastic soils, which were initially unsaturated. In this work we present a back analysis at two different scales on the effects of infiltration into a layer of pyroclastic soils. The evolution of pore water pressure, water content and displacement has been monitored at laboratory scale in a flume test and in situ in the Cervinara slope located North-East of Naples.*

1. INTRODUCTION

This paper presents the prediction made by UPC research group as part of a collaborative piece of research undertaken by different universities to benchmark the hydrological response of small-scale physical model and the data from a well-instrumented natural slopes (details see http://www.iwl.unina2.it/). The benchmarking exercise is based on data monitored at two different scales: an infiltration flume test done in controlled laboratory conditions and the monitoring of Cervinara slope under atmospheric conditions. The modelling at the two scales are presented in the paper using a fully coupled thermo-hydro-mechanical model implemented in a finite element code (CODE_BRIGHT[1]).

2. INFILTRATION FLUME TEST

The infiltration flume test is an instrumented mock-up experiment realized on loose granular volcanic ashes from Cervinara, a mountainous area North-eastern of Naples, Italy [2]. The main characteristics of the tests reproduced in this work are reported in Table 1.

The retention curve has been obtained from relationship between degrees of saturation and suctions measured at different depths in test D4 and D3. It is depicted in Figure 1. Once fixed the water retention curve, the hydraulic model has been calibrated by back-analyzing the intrinsic permeability (5.28e-5 m/s) and the relative permeability function from the time evolutions of pore pressure measured in tests D3 and D4.

In order to predict the rainfall-induced displacements and their effects on the hydraulic response of the soil stratum, the hydraulic model has been then coupled to a mechanical constitutive model. An enhanced formulation of the original CASM model, this formulation, developed by Gonzalez[3], includes a dependency of the yield envelope of the material on suction,. An interesting feature of the model is the flexible definition of the shape of the yield envelope, which allows well-reproducing the shear strength of the material on the dry side of the critical state. Table 2 indicate the parameters and the values used for the mechanical behaviour of the soil.

The most important results from model calibration on test D3 are depicted in Figure 2. Figure 2a shows a comparison of suction time evolutions at three tensiometers located respectively at the bottom (T3 and T4) and top (T6) of the soil layer. When infiltration starts, tensiometers T6 registered an early and quick decrease in suction, well-reproduced by the model. Tensiometers T3 and T4 respond also with a sharp decrease in suction but delayed for six minutes with respect to T6. This kind of response indicates the advance of a wetting front, well-captured by the model. In the other hand Figure. 2b present the evolution of surface

settlements obtain whit the model, the model is able to reproduce the response observed and the failure time.

Test	Soil thickness (cm)	Slope length (cm)	Slope inclination	Initial porosity	Rainfall intensity (mm/h)	Initial mean suction (kPa)	Duration of the test (min)
D3	10	100	40º	0.75	55	17.5	36
C4	10	110	40º	0.65	60	52	-

Table 1 Characteristics infiltration flume test

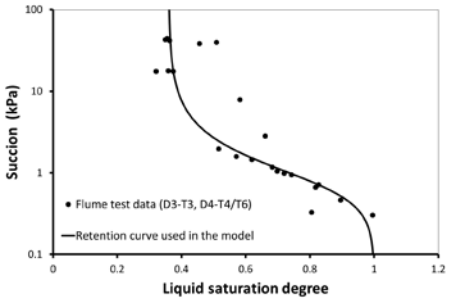

Figure 1 Retention curve of the material used in the mock-up test

υ	κ	λ	r_{casm}	n	M	r	β	Pc	k
0.3	0.04	0.135	2	2	1.54	0.6	37	$1.\ 10^{-15}$	0

Table 2 Mechanical parameters of the material used in the mock-up test

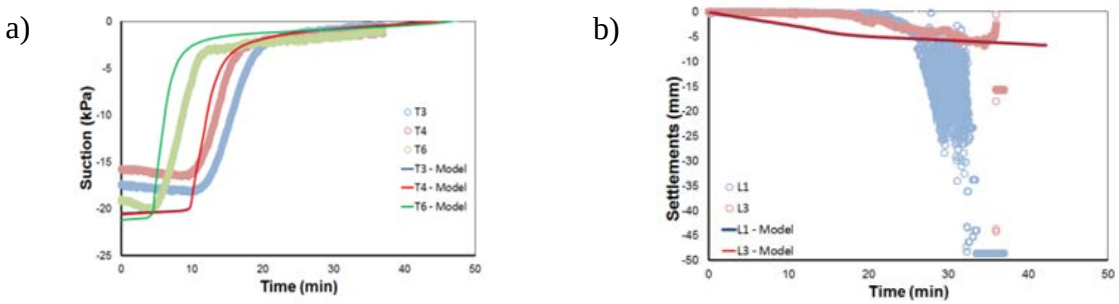

Figure 2 Small-scale model calibration: a) time evolution of suction at three tensiometers b) time evolution surface settlements

The back-analyzed parameters have been used for the Round Robin test, which consists in predicting the hydro-mechanical response of test C4. According to Table 1, the density of the sample in this test is higher than that of test D3. Permeability and preconsolidation pressure have been consequently corrected according to the Kozeny equation and material virgin compression curve. A value of k=1.76e-5 m/s had been then used for test C4.

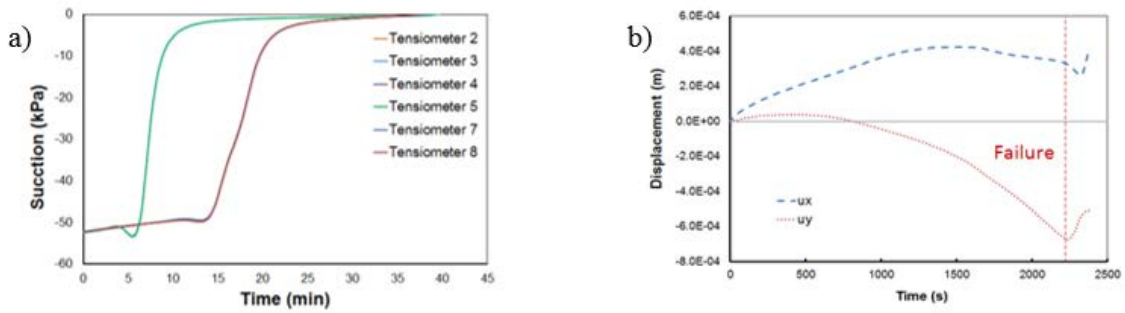

Figure 3 Small-scale model prediction a) Suction evolution b) Displacement evolution

Predicted evolution of suction for test C4 at different depths is shown in Fig.3.a. As a result of the lower permeability, the velocity of the wetting front is lower and the delay between top

and bottom tensiometers response is higher than in test D3. Fig. 3.b shows the evolution of settlement with time. Model predicts infiltration-induced collapse deformation up to 37 mins. At that time, evolution trends changes and a sudden dilation is predicted in the sample. Two minutes after, program stops converging. The moment of dilation initiation is considered as being the one at which failure takes place, 37 mins.

3. FIELD EXPERIMENT

The field experiment considered in the Round Robin contest is the Cervinara slope, a monitored slope under atmospheric actions located North-East of Naples[4] monitored variables include volumetric water content and matric suction at different depths.

The calibration data, provided consist in the field measures recorded from January to August 2011. Meteorological record over the year 2011is shown in Figure 4a. In a general view of the slope lithology, and only for a sake of the prediction of the hydraulic response, the ground has been simplified into a four-strata column of 5 m high (see Figure 4b). One of the most interesting characteristics of this site is the effect that an aquifer located in the bedrock generates in the superior layer, this effect is simulated by a particular boundary condition at the bottom, additionally a special boundary conditions that captures the main mass and heat fluxes due to ground-atmosphere interactions imposed at the top.

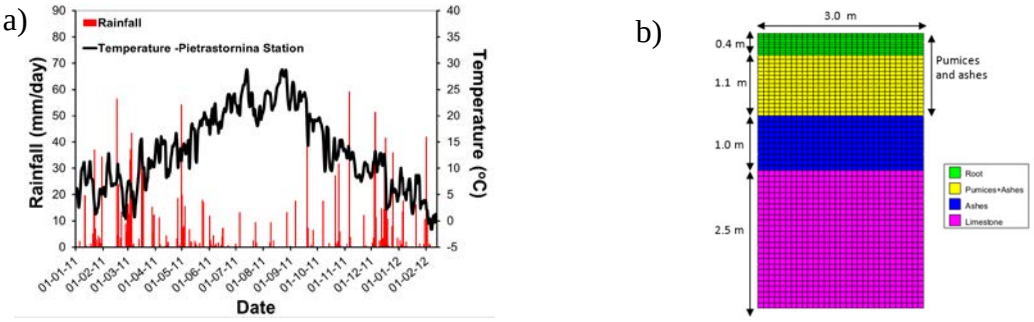

Figure 4 a) Atmospheric data b) Geometry and mesh of the large-scale model

The soil-atmosphere boundary condition implemented in Code-Bright code, accounts for several mass and heat fluxes: rainfall precipitation (P), run-off (R), ponding (Po), evapotranspiration (ET), solar short-wave and long-wave radiation (Rn), ground radiation (Rg), ground reflection (Re), sensible heat (Hs) and heat convected by the mass flux (composed essentially by the latent heat released by evapotranspiration).

The retention curves of the different layers have been estimated on the basis of the relationships drawn by measurements of suction and water content at several depths in the slope. As shown in Figure 5, two water retention curves have been identified: one for slope layers above a depth of 1.5 m, corresponding to the zone of root and pumices ashes, and the second for layers at higher depths, classified as ashes and limestone. Values considered for the intrinsic permeability and porosity for the pyroclastic materials are 5 10^{-5} m/s and 0.7, respectively.

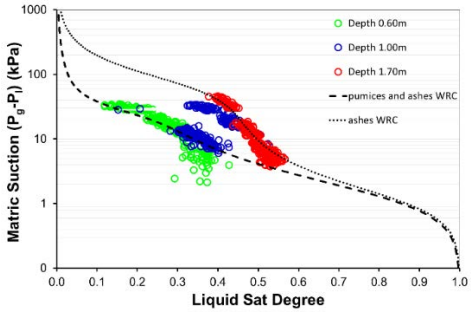

Figure 5 Water retention curve of the different strata

The response output by the model is shown in Figure 7 in terms of suction evolution, the results obtain whit the model agree whit the response observed in the field, with this back analysis results several predictions are made for the rest of the year. The results present that additionally to the atmospheric conditions, that effect imposed by the decreasing of the water level at the aquifer is very important, evidenced in the fact that the suction increasing trend in the deepest tensiometers is steeper than above.

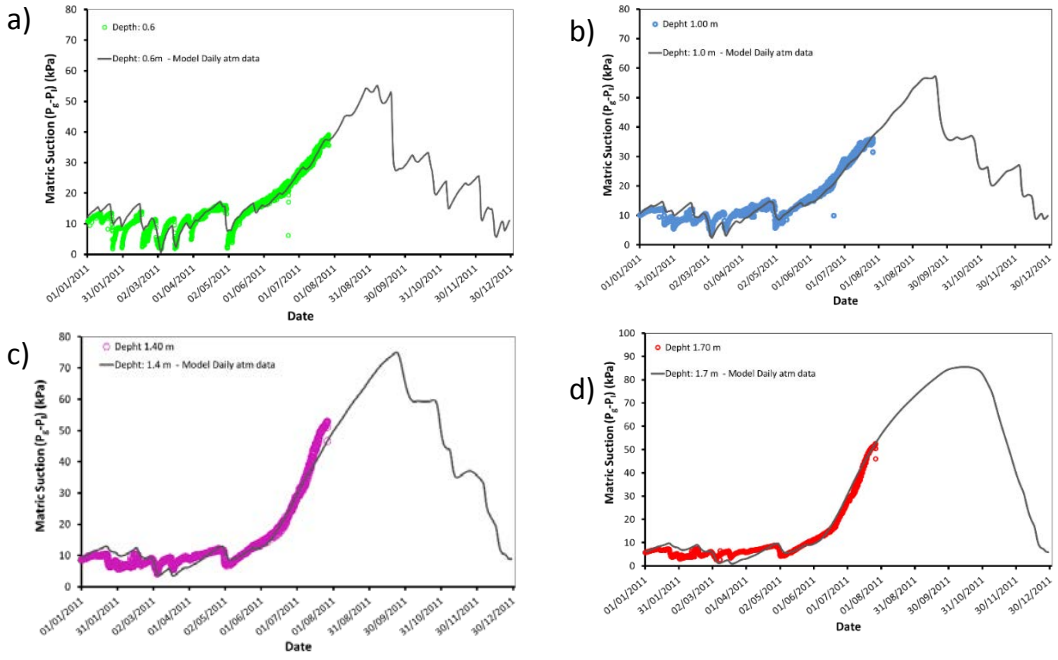

Figure 6 Large-scale model calibration: comparison of computed and measured volumetric water content at a depth of a) 0.30 m, b) 0.60 m, c) 1.00 m and d) 1.70 m

4. CONCLUSIONS

The numerical analyses of the hydro-mechanical response of two slopes in pyroclastic soils has been carried out at two different scales using a thermo-hydro-mechanical Finite Element code that includes a special boundary condition to simulate the ground-atmosphere interactions. The model well predicts the evolution of suction at different depths, surface settlement and time of failure of a mock-up test that simulate the failure of a 40º slope under rainfall. The soil-atmosphere formulation is based on a consistent thermo-hydro-mechanical framework based upon fundamental physics. The model proves to provide good predictions of suction and water content variations in a real slope meteorological actions.

5. REFERENCES

1. Olivella, S., Gens, A., Carrera, J. & Alonso, E. E. Numerical formulation for a simulator (CODE_BRIGHT) for the coupled analysis of saline media. *Eng. Comput.* **13,** 87–112 (1996).
2. Greco, R., Guida, a., Damiano, E. & Olivares, L. Soil water content and suction monitoring in model slopes for shallow flowslides early warning applications. *Phys. Chem. Earth, Parts A/B/C* **35,** 127–136 (2010).
3. González, N. Development of a family of constitutive models for geotechnical applications. 47–84 (2011).
4. Damiano, E., Olivares, L. & Picarelli, L. Steep-slope monitoring in unsaturated pyroclastic soils. *Eng. Geol.* **137-138,** 1–12 (2012).

Implementation in CODE_BRIGHT of triangle elements between tetrahedron elements for flow and transport

Sebastia Olivella, Geotechnical and Geosciences Department, Escola de Camins, UPCBarcelonaTech

Abstract

This paper presents the finite element formulation for a 2D triangle to be incorporated into a 3D mesh composed by tetrahedral elements. The element connects nodes on the tetrahedral faces and permits to simulate mass and heat conservation problems in fractured media.

Introduction

A way to simulate mass and heat flow through fractures in a rock is to incorporate 2D elements in 3D finite element meshes. When a fracture is represented by two parallel surfaces the generated finite elements are very small. Essentially their size is the thickness of the fracture, and distorted elements lead to numerical difficulties. Using parallel surfaces may seriously compromise the possibility to develop a realistic mesh specially if the actual thickness of the fracture is to be represented. Including planar elements characterized provides an interesting solution. For a tetrahedral mesh, triangles between them can be implemented. The same happens in 2D problems for which 1D elements (segments) can be implemented.

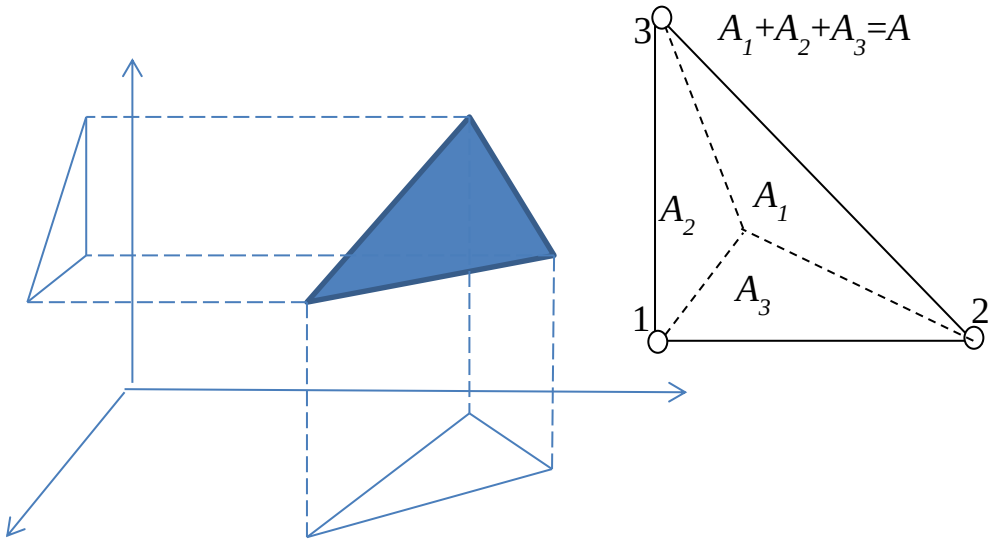

Figure 1. Triangle in 3 dimensions and areas associated to nodes to be used to define interpolation functions.

Development of isoparametric shape functions

In a tetrahedral mesh, a discontinuity can be represented by triangular elements as has been indicated. The planar element requires properties that can be integrated in a certain thickness such as transmissivity which is calculated as the product of the thickness and the permeability. Figure 1 shows a triangle element in a 3-D space. The isoparametric interpolation function for a triangle in space can be defined using the areal coordinates, which are defined as:

$$L_1 = \frac{A_1}{A} \qquad L_2 = \frac{A_2}{A} \qquad L_3 = \frac{A_3}{A} \tag{1}$$

The area of the triangle is calculated using the modulus of the vector product of the following two vectors:

$$\mathbf{v}_{12} = \begin{pmatrix} x_2 - x_1 & y_2 - y_1 & z_2 - z_1 \end{pmatrix} \qquad \mathbf{v}_{13} = \begin{pmatrix} x_3 - x_1 & y_3 - y_1 & z_3 - z_1 \end{pmatrix} \tag{1}$$

as the modulus of the vector product corresponds to 2 times the area of the triangle. The vector product is:

$$2A = \operatorname{mod}\left(\mathbf{v}_{12} \times \mathbf{v}_{13}\right) = \operatorname{mod}\begin{vmatrix} i & j & k \\ x_2 - x_1 & y_2 - y_1 & z_2 - z_1 \\ x_3 - x_1 & y_3 - y_1 & z_3 - z_1 \end{vmatrix} = \operatorname{mod}\left[a_i i + a_j j + a_k k\right] \tag{2}$$

The area of the triangle can be therefore expressed directly as:

$$A = \frac{1}{2}\sqrt{a_i^2 + a_j^2 + a_k^2} \quad \text{where} \quad a_i = \left[\left(y_2 - y_1\right)\left(z_3 - z_1\right) - \left(z_2 - z_1\right)\left(y_3 - y_1\right)\right] \tag{3}$$

$$a_j = \left[-\left(x_2 - x_1\right)\left(z_3 - z_1\right) + \left(z_2 - z_1\right)\left(x_3 - x_1\right)\right] \qquad a_k = \left[\left(x_2 - x_1\right)\left(y_3 - y_1\right) - \left(y_2 - y_1\right)\left(x_3 - x_1\right)\right]$$

The same equations can be applied to a triangle formed by nodes 2 and 3 and any point (x, y, z) inside the triangle. With the area defined by the internal point and two nodes, the areal coordinate of the point (x, y, z) is defined as:

$$L_1 = \frac{A_1}{A} \tag{4}$$

for which A_1 is obtained from the vector product modulus of the following two vectors:

$$\mathbf{v}_{x2} = \begin{pmatrix} x_2 - x & y_2 - y & z_2 - z \end{pmatrix} \qquad \mathbf{v}_{x3} = \begin{pmatrix} x_3 - x & y_3 - y & z_3 - z \end{pmatrix} \tag{5}$$

Which is expressed as:

$$2A_1 = \operatorname{mod}\left(\mathbf{v}_{x2} \times \mathbf{v}_{x3}\right) = \operatorname{mod}\begin{vmatrix} i & j & k \\ x_2 - x & y_2 - y & z_2 - z \\ x_3 - x & y_3 - y & z_3 - z \end{vmatrix} = \operatorname{mod}\left[a_{i1} i + a_{j1} j + a_{k1} k\right] \tag{6}$$

So, the area of the triangle can be written directly as:

$$A_1 = \frac{1}{2}\sqrt{a_{i1}^2 + a_{j1}^2 + a_{k1}^2} \qquad \text{where} \qquad a_{i1} = \left[(y_2 - y)(z_3 - z) - (z_2 - z)(y_3 - y)\right] \tag{7}$$

$$a_{j1} = \left[-(x_2 - x)(z_3 - z) + (z_2 - z)(x_3 - x)\right] \qquad a_{k1} = \left[(x_2 - x)(y_3 - y) - (y_2 - y)(x_3 - x)\right]$$

And the areal coordinates which in fact are used as interpolation functions are:

$$N_1 = L_1 = \frac{A_1}{A} = \frac{\sqrt{a_{i1}^2 + a_{j1}^2 + a_{k1}^2}}{\sqrt{a_i^2 + a_j^2 + a_k^2}} \tag{8}$$

For every node of the triangle the same calculation is done and this means that it can be written in general as:

$$L_m = \frac{A_m}{A} = \frac{\sqrt{a_{im}^2 + a_{jm}^2 + a_{km}^2}}{\sqrt{a_i^2 + a_j^2 + a_k^2}} \tag{9}$$

$$\begin{pmatrix} \frac{\partial L_m}{\partial x} & \frac{\partial L_m}{\partial y} & \frac{\partial L_m}{\partial z} \end{pmatrix} = \frac{1}{4AA_m}\begin{pmatrix} a_{im} & a_{jm} & a_{km} \end{pmatrix}\begin{pmatrix} \frac{\partial a_{im}}{\partial x} & \frac{\partial a_{im}}{\partial y} & \frac{\partial a_{im}}{\partial z} \\ \frac{\partial a_{jm}}{\partial x} & \frac{\partial a_{jm}}{\partial y} & \frac{\partial a_{jm}}{\partial z} \\ \frac{\partial a_{km}}{\partial x} & \frac{\partial a_{km}}{\partial y} & \frac{\partial a_{km}}{\partial z} \end{pmatrix} \tag{10}$$

$$\begin{aligned} a_{i1} &= \left[(y_2 - y)(z_3 - z) - (z_2 - z)(y_3 - y)\right] \\ a_{j1} &= \left[-(x_2 - x)(z_3 - z) + (z_2 - z)(x_3 - x)\right] \\ a_{k1} &= \left[(x_2 - x)(y_3 - y) - (y_2 - y)(x_3 - x)\right] \end{aligned} \qquad \begin{bmatrix} \frac{\partial a_{i1}}{\partial x} & \frac{\partial a_{j1}}{\partial x} & \frac{\partial a_{k1}}{\partial x} \\ \frac{\partial a_{i1}}{\partial y} & \frac{\partial a_{j1}}{\partial y} & \frac{\partial a_{k1}}{\partial y} \\ \frac{\partial a_{i1}}{\partial z} & \frac{\partial a_{j1}}{\partial z} & \frac{\partial a_{k1}}{\partial z} \end{bmatrix} = \begin{bmatrix} 0 & z_3 - z_2 & y_2 - y_3 \\ z_2 - z_3 & 0 & x_3 - x_2 \\ y_3 - y_2 & x_2 - x_3 & 0 \end{bmatrix} \tag{11}$$

$$\begin{aligned} a_{i2} &= \left[(y_3 - y)(z_1 - z) - (z_3 - z)(y_1 - y)\right] \\ a_{j2} &= \left[-(x_3 - x)(z_1 - z) + (z_3 - z)(x_1 - x)\right] \\ a_{k2} &= \left[(x_3 - x)(y_1 - y) - (y_3 - y)(x_1 - x)\right] \end{aligned} \qquad \begin{bmatrix} \frac{\partial a_{i2}}{\partial x} & \frac{\partial a_{j2}}{\partial x} & \frac{\partial a_{k2}}{\partial x} \\ \frac{\partial a_{i2}}{\partial y} & \frac{\partial a_{j2}}{\partial y} & \frac{\partial a_{k2}}{\partial y} \\ \frac{\partial a_{i2}}{\partial z} & \frac{\partial a_{j2}}{\partial z} & \frac{\partial a_{k2}}{\partial z} \end{bmatrix} = \begin{bmatrix} 0 & z_1 - z_3 & y_3 - y_1 \\ z_3 - z_1 & 0 & x_1 - x_3 \\ y_1 - y_3 & x_3 - x_1 & 0 \end{bmatrix} \tag{12}$$

$$\begin{aligned} a_{i3} &= \left[(y_1 - y)(z_2 - z) - (z_1 - z)(y_2 - y)\right] \\ a_{j3} &= \left[-(x_1 - x)(z_2 - z) + (z_1 - z)(x_2 - x)\right] \\ a_{k3} &= \left[(x_1 - x)(y_2 - y) - (y_1 - y)(x_2 - x)\right] \end{aligned} \qquad \begin{bmatrix} \frac{\partial a_{i3}}{\partial x} & \frac{\partial a_{j3}}{\partial x} & \frac{\partial a_{k3}}{\partial x} \\ \frac{\partial a_{i3}}{\partial y} & \frac{\partial a_{j3}}{\partial y} & \frac{\partial a_{k3}}{\partial y} \\ \frac{\partial a_{i3}}{\partial z} & \frac{\partial a_{j3}}{\partial z} & \frac{\partial a_{k3}}{\partial z} \end{bmatrix} = \begin{bmatrix} 0 & z_2 - z_1 & y_1 - y_2 \\ z_1 - z_2 & 0 & x_2 - x_1 \\ y_2 - y_1 & x_1 - x_2 & 0 \end{bmatrix} \tag{13}$$

Example of application

A simple calculation has been carried out to illustrate the presence of 2D elements with large transmisivity in a 3D domain. The results in figure 2 can correspond to piezometric head or pressure (in this second case, gravity is neglected).

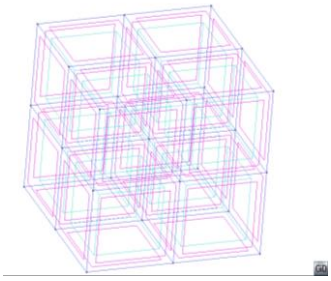

Geometry

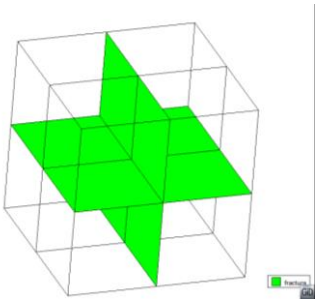

fractures

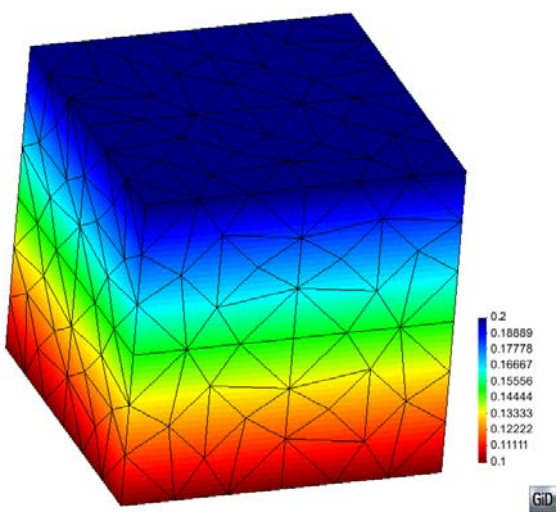

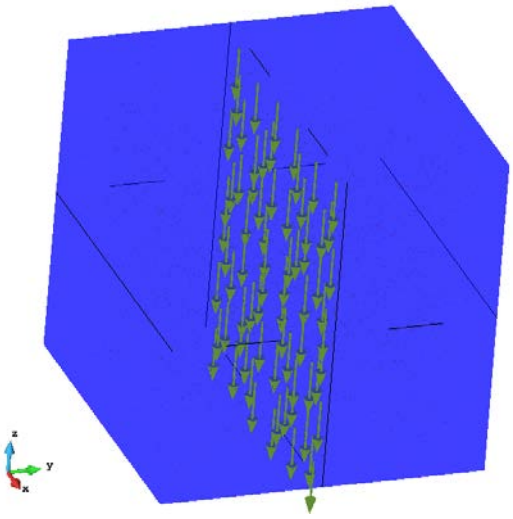

Figure 2. Variable distribution in a block and corresponding flux field.

Conclusions

This element can be very useful to model fractured media under non-isothermal conditions. If the mechanical part is solved, this element can be excluded for the stiffness contribution.

LONGITUDINAL DEFORMATION PROFILES OF TUNNELS EXCAVATED IN STRAIN-SOFTENING ROCK MASSES

Alfonso Rodriguez-Dono[1], Leandro R. Alejano[2] and María Veiga[3]

[1] Ph.D. Mining Engineer. Department of Geotechnical Engineering and Geosciences
Universitat Politècnica de Catalunya (UPC). e-mail: alfonso.rodriguez@upc.edu

[2] Ph.D. Mining Engineer. Department of Natural Resources and Environmental Engineering
Universidade de Vigo e-mail: alejano@uvigo.es

[3] Itasca Consultants AB, Stockholm, Sweden.

Key words: Convergence-confinement, strain-softening, longitudinal deformation profile

Abstract. *We describe techniques to estimate longitudinal deformation profiles of tunnels excavated in rock masses. The longitudinal deformation profile, a graph that relates a fictitious internal pressure to the distance to the tunnel face, is necessary to assess adequate distance to the face for the purpose of installing support. Traditional application of this method usually relies on an elastic representation of the longitudinal deformation profile. A more realistic approach has been proposed recently that accounts for the elastoplastic nature of rock masses. It is based, however, on assuming elastic–perfectly plastic rock mass behaviour, an assumption which is more or less realistic, but only for low quality rock masses with a geological strength index (GSI) below 35. We extend this approach to the case of strain-softening rock masses representing a wider range of rock masses (25 < GSI < 75). Based on studying various numerical techniques to estimate these curves, we propose a simplified approximate equation of the plastic radius of a tunnel excavated in a strain-softening rock mass, which can be combined with existing longitudinal deformation profile estimation techniques to analytically obtain a more realistic approach to calculating longitudinal deformation profiles for strain-softening rock masses.*

1 INTRODUCTION

The convergence-confinement method is an approach to analyzing stress–strain problems in tunnels that provides a general albeit simplified estimate of the nature of the interplay between the rock mass and support installed at a distance from the face. When the support is installed close to the tunnel face, it does not carry the full load to which it will be subjected once the tunnel face has moved. The face itself carries a significant portion of the load of its surroundings.[i]

The three basic components of the convergence-confinement method are the ground reaction curve (GRC), the support characteristic curve (SCC) and the longitudinal deformation profile (LDP). The LDP is a graphical representation of radial displacement (tunnel wall deformation) versus distance to the tunnel face for an unsupported tunnel section, behind and ahead of the tunnel face, along the tunnel axis. An accurate description of the LDP is needed to estimate optimal distance of the support from the face. The LDP and the GRC both strictly depend on the characteristics of the rock mass to be excavated, whereas the SCC and support distance from the face have to be designed bearing in mind the particular needs of the section to be excavated.

Starting from the 1970s, different rigorous solutions to accurately calculating GRCs have been proposed for different types of rock behaviour models, including elastic–perfectly plastic (EPP) materials, elastic-brittle (EB) materials and strain-softening (SS) materials. It is also possible to use plane-strain 2D numerical models in which mesh dependency can be observed in particular circumstances. As has been demonstrated by the authors elsewhere,[ii] rock mass response will differ depending on the behavior model selected.

In the early years of application of the convergence-confinement method, the LDP was usually calculated elastically. In-place measurements, however, showed that this elastic approach was inaccurate, especially in large deformation conditions. Recently, Vlachopoulos and Diederichs[iii] have proposed a robust formulation, based on a number of numerical models, to estimate the LDP according to the significant influence of the ultimate plastic radius, shown to play a definitive role in the development and shape of the LDP.

Vlachopoulos and Diederichs considered that materials in rock masses that had attained maximum strength are able to retain the stress level for further deformation; in other words, these are EPP rock masses. This behaviour model, however, does not seem to properly model the behaviour of average to good quality rock masses, which are considered to exhibit SS behavior.[iv] The plastic zone around excavations tends to be larger for SS rock masses compared to EPP rock masses. For this reason we focus, in this study, on extending the Vlachopoulos and Diederichs approach to SS behaviour.

Sole application of the GSI is largely questionable as a rock mass characterisation method, so we highly recommend further studies for particular tunnelling applications: RQD, RMR, Q, discontinuity data collection and detailed geological and hydrogeological studies. Nonetheless, the GSI system is convenient within the scope of our study, as it reflects general rock mass quality (joint density and joint strength behaviour) in a simple way and so enables us to easily assign a concrete behaviour model to the rock mass and estimate its parameters.

2 NUMERICAL CALCULATION OF LDPS IN SS ROCK MASSES

In this section we analyse how SS behaviour affects LDPs in tunnels. Following Vlachopoulos and Diederichs, several FLAC models were used to tunnel a series of rock masses of decreasing rock mass quality. To highlight differences, the models reflected very deep tunnels excavated in low strength rock. Simulations were run using both Hoek–Brown and Mohr–Coulomb parameters. The rock masses were characterised following a procedure developed by the authors[v] with the help of RocLab.[vi] Using these techniques, the equivalent Hoek–Brown and Mohr–Coulomb strength parameters were obtained.

The Hoek–Brown SS rock mass model, as implemented in both FLAC2D and FLAC3D codes, had an associated flow rule adapted to the failure criterion; hence, dilatancy could not be explicitly included. However, the Mohr–Coulomb models were run to analyse the role of dilatancy in LDPs. All the models were run for both the Hoek–Brown and Mohr–Coulomb cases and similar results were obtained.

Neumann boundary conditions were used for the FLAC2D models, that is, stresses were fixed at some model boundaries; meanwhile, Dirichlet boundary conditions were used for the FLAC3D models, that is, all boundary displacement was fixed (except in the excavated tunnel surface), and the field stress was initialized in the entire discretized area. As was anticipated, the displacements indicated by the FLAC2D models were slightly larger than those predicted by the FLAC3D models—a difference we attribute to the boundary conditions (Figure 1).

We propose using SS LDPs in applying the convergence-confinement method in average

to high quality rock masses. The rock mass can be characterised following Hoek and Brown (1997) and Alejano et al. (2010); the LDPs can be obtained according to Vlachopoulos and Diederichs (2009); the plastic radius can be obtained using the estimation proposed in Alejano et al. (2012)[vii]; and the GRC can be estimated according to any of the more or less simplified but rigorous numerical approaches existing in the literature. This proposal relies on the fact that, as shown in Figure 2, the use of an LDP based on EPP behaviour when dealing with rock masses with SS behaviour underestimates displacement when support or reinforcement is installed, leading to inappropriate and potentially inaccurate designs.

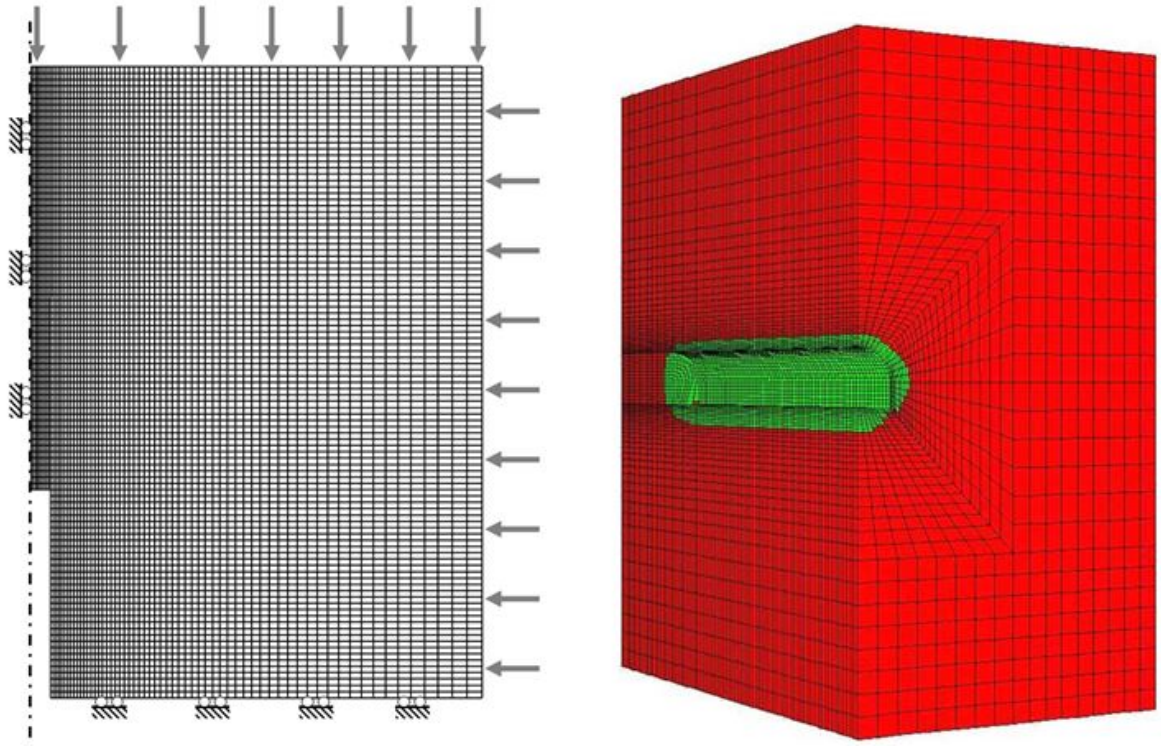

Figure 1. Meshes used for the numerical modelling. (a) Mesh used for the FLAC2D models. (b) Example of a tunnel modelled in FLAC3D to analyse longitudinal deformation profiles (LDP). The green color indicates the plastic zone around the tunnel.

Note that, even for a stable tunnel face, such inaccuracies may result in higher closure rates and a loss of rock strength. For instance, in some tunnels in very deformable rock, support must be installed early on in order to ensure a safe working environment at the face; however, it is preferable to delay full reinforcement to prevent an unacceptable build-up of internal loads due to high closure rates near the face. Premature installation of the final lining based on an EPP approach to estimating LDP (Figure 2) could result in buckling of the primary support system, expansion of the plastic zone and an increase in final closure.[viii]

3 CONCLUSIONS

Some of the limitations of the convergence-confinement method relate to the knowledge of actual rock behaviour. One such issue is the correct definition of post-failure behaviour in the rock mass, which has a bearing on rock mass behaviour in the plastic zone. Once post-failure behaviour is defined, it is still necessary to adequately characterise SS rock masses. And once all the rock mass parameters are known, suitable tools are needed to provide reliable designs.

To establish the appropriate LDP for the tunnel is very important for estimating suitable timing for support installation. The use of an inappropriate LDP can produce significant errors in calculating the support installation distance from the tunnel face, likely to produce failure or problems with support systems.

We have extended previous approaches to estimating the LDPs for tunnels excavated in EPP material to the case of SS material, representing a wider range of rock masses (25 < GSI < 75). Our simplified approximate equation for the plastic radius of a tunnel excavated in a SS rock mass analytically obtains a more realistic LDP calculation for tunnels excavated in average quality rock masses.

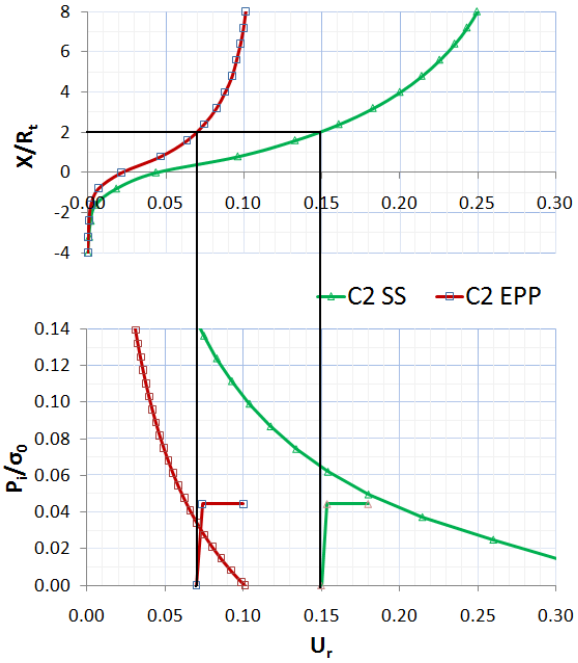

Figure 2. Application of the convergence-confinement method to a tunnel. Typical graphs obtained of the GRC and SCC (below) and LDP (above). Red indicates the elastic–perfectly plastic (EPP) approach and green indicates the strain-softening (SS) approach. Note that although the tunnel would be correctly stabilised in the EPP case, in the SS case the lining would be unable to withstand the ground load.

REFERENCES

[i] Carranza-Torres, C., Fairhurst, C., 2000. Application of convergence-confinement method of tunnel design to rock masses that satisfy the Hoek–Brown failure criterion. Tunn. Undergr. Sp. Technol. 15 (2), 187–213.

[ii] Alejano, L.R.,Rodriguez-Dono,A., Alonso,E., Fernández-Manín, G., 2009. Ground reaction curves for tunnels excavated in different quality rock masses showing several types of post-failure behaviour. Tunn. Undergr. Sp. Technol. 24 (6), 689–705.

[iii] Vlachopoulos, N., Diederichs, M.S., 2009. Improved longitudinal displacement profiles for convergence confinement analysis of deep tunnels. Rock Mech. Rock Eng. 42 (1), 131–146.

[iv] Hoek, E., Brown, E.T., 1997. Practical estimates of rock mass strength. Int. J. Rock Mech. Min. Sci. 34 (8), 1165–1186.

[v] Alejano, L.R., Alonso, E., Rodriguez-Dono, A., Fdez-Manín, G., 2010. Application of the convergence-confinement method to tunnels in rock masses exhibiting Hoek–Brown strain-softening behaviour. Int. J. Rock Mech. Min. Sci. 47 (1), 150–160.

[vi] Rocscience, 2003. RocLab. Rocscience Inc., Toronto, Canada. <www.rocscience.com>.

[vii] Alejano LR, Rodriguez-Dono A, Veiga M. Plastic radii and longitudinal deformation profiles of tunnels excavated in strain-softening rock masses. Tunnel Underground Space Technol. 2012;30:169–82.

[viii] Hoek, E., Carranza-Torres, C., Diederichs, M., Corkum, B., 2008. The 2008 Kersten lecture integration of geotechnical and structural design in tunnelling. In: 56th Annual Geotechnical Engineering Conference, 2008. University of Minnesota, USA.

IMPLICIT STRESS INTEGRATION OF THE BARCELONA BASIC MODEL IN LAGAMINE

A.C. Dieudonne[*,†], F. Collin[*], S. Levasseur[*], R. Charlier[*]

[*] ArGEnCo Department
University of Liege (ULg)
Chemin des Chevreuils 1, 4000 Liege, Belgium
e-mail: ac.dieudonne@ulg.ac.be

[†] F.R.I.A., Fonds de la Recherche Scientifique – FNRS
Rue d'Egmont 5, 1000 Brussels, Belgium

Key words: Barcelona Basic Model, Elasto-plasticity, Implicit stress integration

Abstract. *The paper presents the stress integration scheme used for the implementation of the Barcelona Basic Model in the finite element code Lagamine. The proposed scheme is based on the return mapping algorithm with a backward Euler (fully implicit) time discretization. The accuracy of the stress-strain integration is improved by using a sub-stepping procedure. Verification of the model implementation within the elastic domain is provided by comparing the numerical responses of the model along various stress paths with the corresponding analytical solutions. Additionally, the numerical responses over the whole stress range are compared to the ones provided by Alonso et al. (1990)*[i].

1 INTRODUCTION

In the last decades, particular attention has been paid to the behaviour of compacted clays, especially in relation to their use as engineered barriers in deep geological repositories for nuclear waste. The Barcelona Basic Model[i] (Figure 1) is one of the first elastoplastic models developed to describe the behaviour of unsaturated clays. Although other constitutive models were later developed, they generally keep the core of the Barcelona Basic Model (BBM) which has become a reference model in the field of unsaturated soil mechanics.

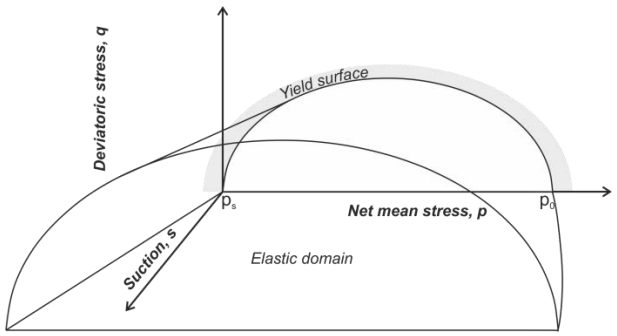

Figure 1: Three-dimensional representation of the yield surfaces in the BBM[i]

The Barcelona Basic Model was implemented in the finite element code Lagamine[ii] which has been developed at the University of Liege. Lagamine is a general-purpose code able to deal with complex non-linear constitutive models, multiphysical coupling, multiscale approaches and strain localization in the fields of metal forming, reservoir engineering and environmental geotechnics.

2 NUMERICAL INTEGRATION IN LAGAMINE

The Barcelona Basic Model is formulated in the form of incremental relationships between stress and strains. Given known incremental displacements or strains (which are given as input of the routine), the integration routine aims at integrating numerically the constitutive relationships in order to update the stresses at integration points.

Integration schemes are generally divided into implicit and explicit algorithms, depending if the stress increment is computed using the stiffness at the start or at the end of each step. An implicit scheme, based on the work of Collin[iii] et al., was used for the implementation of the Barcelona Basic Model in Lagamine. Its main features are presented in this section.

2.1 Objectivity of the stress tensor

In large deformation analysis, the incremental formulation requires to define an objective stress rate. Indeed the stress rate should be frame independent, so that any rigid-body motion does not induce stress within the material. Here, the objectivity of the stress tensor is satisfied by adopting the Jaumann objective stress rate which is introduced before integration of the stress-strain constitutive relationships.

2.2 Return mapping algorithm

The return mapping algorithm is based on an elastic predictor and an eventual plastic corrector if the yield criterion is violated (Figure 2). First, an elastic trial stress state (point E) is computed assuming a purely elastic behaviour (the plastic flow is frozen). If the elastic predictor does not violate the yield criterion, then the updated stress state is obtained (Figure 2a). On the other hand, if the yield criterion is violated, a plastic corrector should be applied to return back on the (updated) yield surface (Figure 2b). The updated stress state is on the yield surface (point B). Different techniques exist to return back on the yield surface. The closest-point projection method is used.

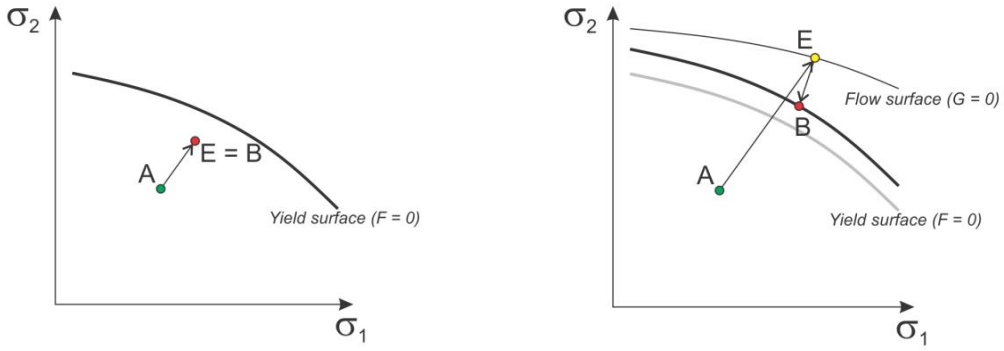

(a) (b)

Figure 2: Return mapping algorithm. (a) The yield criterion is not vioalted. The updated stresses are given by the elastic predictor. (b) The yield criterion is violated. A plastic corrector should be applied to return back on the yield surface and update the stresess.

2.3 Mixed control

The Barcelona Basic Model is formulated in terms two stress variables, namely net stress and suction. However, in most conventional finite element codes (such as Code_Brigh or Lagamine), the increment of suction is given as input of the integration routine, like increment of displacements are. Vaunat et al.[iv] introduced generalized stress and strain variables and presented an implicit stress integration scheme with mixed control, where the constitutive equations are driven partly by the strains (suction) and partly by the stresses (mechanical stresses). Such a formulation is used for the integration of the BBM in Lagamine.

2.4 Sub-stepping procedure

During large time steps where yielding occurs, difficulties may appear in returning back to the yield surface. In such situations, a possible strategy is to use smaller time steps in the global resolution algorithm. However, this solution is not reasonable since the most restrictive integration point will control the global problem. An alternative approach consists in subdividing locally the current time step into several substeps (which can be different for each integration point).

A sub-stepping procedure is used in the integration of the Barcelona Basic Model within Lagamine. A time step Δt is divided into $NINTV$ sub-steps, such as $\delta t = \Delta t / NINTV$. The value of $NINTV$ may either be constant, or computed according to the current normal strain rate.

3 VERIFICATION

The verification process consists in controlling that a computational model accurately represents the underlying mathematical model. In order to verify the stress integration of the Barcelona Basic Model, the response of the model along various stress paths were compared to the corresponding analytical solutions within the elastic domain. An example of such a procedure is shown in Figure 3 for a wetting path under oedometer conditions (constant vertical stress). Additionally, the numerical responses over the whole stress range were compared to the ones provided by Alonso et al. (1990)[i].

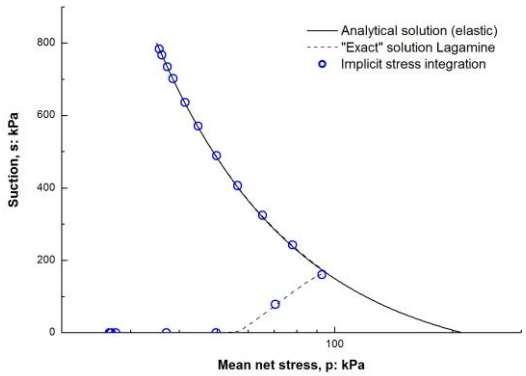

Figure 3: Verification of the model response along wetting under oedometer conditions (constant vertical stress) with the corresponding analytical solution in the elastic domain. The "exact" solution Lagamine refers to the answer of the model obtained for very small loading steps.

4 CONCLUSIONS

The Barcelona Basic Model was implemented within the finite element code Lagamine using a fully implicit stress integration scheme. The implementation was verified using analytical solutions within the elastic domain and compared to responses provided in the literature.

ACKNOWLEDGEMENTS

The first Author wishes to acknowledge Benjamin Cerfontaine from the University of Liege for the fruitful discussions.

REFERENCES

[i] Alonso, E.E., A. Gens, A. Josa, 1990. A constitutive model for partially saturated soils. Géotechnique, 40, 405:430.

[ii] Charlier, R., 1987. Approche unifiée de quelques problèmes non-linéaires de mécanique des milieux continus par la méthode des éléments finis. PhD thesis, University of Liege, 302 p.

[iii] Collin, F., Y.J. Cui, C. Schroeder, R. Charlier, 2002. Mechanical behaviour of Lixhe chalk partially saturated by oil and water: experiment and modelling. International Journal for Numerical and Analytical Methods in Geomechanics, 26, 897:924.

[iv] Vaunat, J., J.C. Cante, A. Ledesma, A. Gens, 2000. A stress point algorithm for an elastoplastic model in unsaturated soils. International Journal of Plasticity, 16, 121:141.

NUMERIC MODELLING IN UDEC OF THE TINYAG MINE EXPLOITATION

Alfonso Rodriguez-Dono[1], Leandro R. Alejano[2] and David Cordova[3]

[1] Ph.D. Mining Engineer. Department of Geotechnical Engineering and Geosciences
Universitat Politècnica de Catalunya (UPC). e-mail: alfonso.rodriguez@upc.edu

[2] Ph.D. Mining Engineer. Department of Natural Resources and Environmental Engineering
Universidade de Vigo e-mail: alejano@uvigo.es

[3] DCR Ingenieros SL (Mining and civil geomechanics company).
C/Altamira 124 urb. Camino Real. La Molina. Lima 12. Peru.

Key words: Numeric modelling, UDEC, sublevel caving, failure, subsidence

Abstract. *The aim of this paper is to perform a simplified numeric model of the labours in the Tinyag underground mining exploitation (sublevel caving method), in order to estimate the possible behaviour of the rock mass affected by the labours, and to detect possible failure mechanisms (circular failure, toppling, etc.). The model is also interesting to identify the subsidence mechanisms associated and to have an approximate vision of the existent geomechanical risks. We have performed this model using UDEC.*

1 INTRODUCTION

The Tinyag mine is located in the Peruvian Andes, at 4700 m.a.s.l. The upper part of the deposit has been exploited by means of opencast mining. This exploitation has already been concluded because it reached the economic limit. Below that elevation, it is planned to continue the exploitation by means of underground mining, using the sublevel caving method. Tinyag is a semi-tabular deposit, 200 m long and 15-25 m thick. The ore is scattered in a skarn, forming sulphide massive bodies, mainly Zn (7.7 %).

The aim of this work is to carry out a simplified numeric model of the labours in the Tinyag underground mining exploitation, in order to estimate the possible behaviour of the rock mass affected by the labours and to detect possible failure mechanisms. The model is also interesting to identify the subsidence mechanisms associated to the sublevel caving method. We think the numeric model can be an important contribution to achieve these goals.

We have used UDEC (Universal Distinct Element Code), developed by Itasca[1], to carry out this model. UDEC is a numeric code based in the discrete elements method. UDEC simulates the behaviour of discontinuous media subjected to loads. The discontinuous medium is represented by means of discrete blocks connections, which can behave as rigid or deformable blocks. Joints and discontinuities are considered as contour conditions between blocks. This allows great block displacements, including its separation and rotation. This is considered one of the main advantages of UDEC among other codes.

This code includes several behaviour models, which make easier the modelling of different materials and geological structures. UDEC is based in lagrangian calculations, very suitable for the simulation of great displacements and deformations in a medium formed by blocks. UDEC is especially suitable to detect physical instabilities in rock mechanics engineering problems, related with open pit or underground mining.

2 MODEL DEVELOPMENT AND RESULTS

We propose a simplified model, developed according to the geological sections and the geometry of the mine. We distinguish 9 different rock masses, plus a rock fill added to the sill (Figure 1). The skarn mineral, the earthy pyrite and the rock fill have been considered as discontinuous material, constituting blocks according to three joint sets, which form angles of 0º, 70º and 110º to the horizontal. The rest of the layers have been modelled as a continuous deformable media.

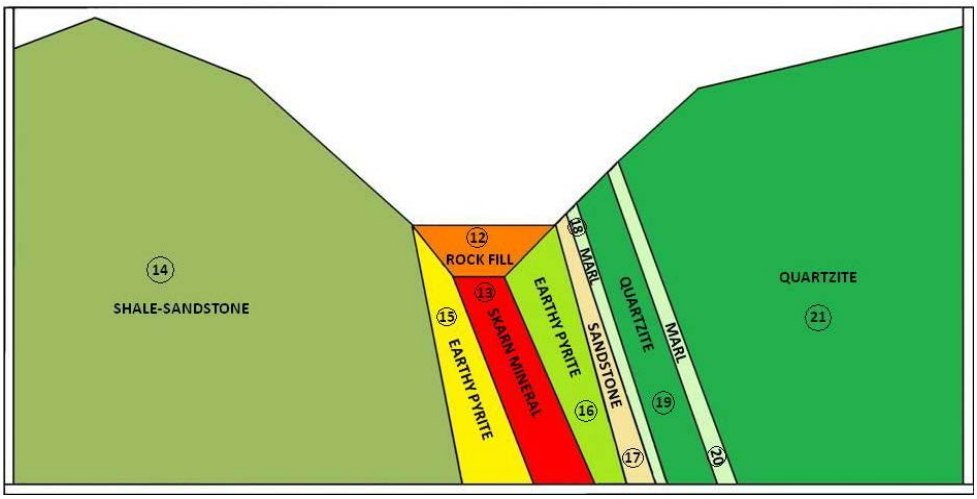

Figure 1. Simplified model of the geological cut of the Tinyag mine

The ore is being extracted in 4 phases. This exploitation will produce a progressive subsidence and affections to the rock mass. The collapse of the blocks takes place as the model is running. These blocks tend to fill the exploited area. At the end of phase 2, a certain subsidence has been produced in the surface. The subsidence phenomena should always be taken into account when the sublevel caving method is used. In the exploitation phase 3 (figures 2 and 3), we can observe that, besides the subsidence, certain toppling begin to take place. We can identify this phenomenon through the cracks and steps produced in the surface. When the model reaches the phase 4 (figure 4), large deformations and large shear stresses are produced. These stresses induce plastic deformations that could give rise to circular failure (red asterisks in figure 4).

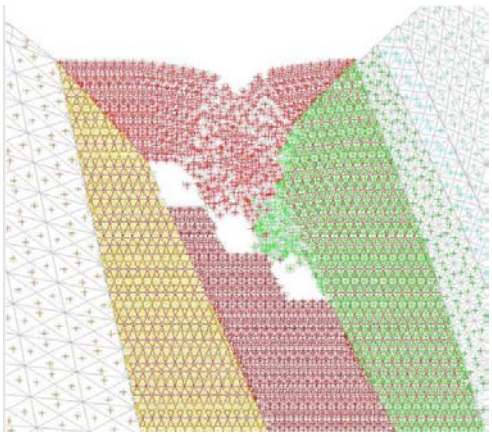

Figure 2. Phase 3 – Beginning

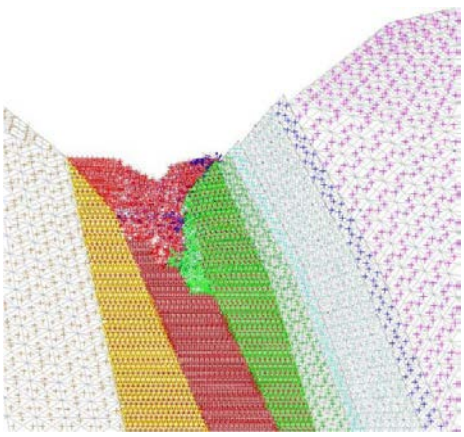

Figure 3. Phase 3 – Ending

3 CONCLUSIONS

A numeric model of the Tinyag mine exploitation, in Peru, has been built with the aid of the UDEC code. The underground mining method selected is the sublevel caving method. The aim of this work is to assess the behaviour of the rock mass affected by the exploitation and to identify the possible failure and subsidence mechanisms that could take place.

In the numeric model, the exploitation has been carried out in 4 phases, and we have been able to observe how the collapse of the rock mass takes place, as described by other authors like Kvapil[ii]. We have observed also that a subsidence occurs in the surface, as it is usual in sublevel caving and as it actually happened in the Tinyag mine, as we can see in figure 5.

Finally, we have observed that toppling of the blocks in the hanging wall could take place and, as a matter of fact, tensile cracks have arisen in the mine wall, as we can see in figure 6. Moreover, we have observed that large shear stresses and large plastic deformations can show up. And we think that these stresses could give rise to a circular-type failure in the hanging wall (figure 4).

Therefore, we believe that the appropriate studies and the adequate actions should be taken to avoid these studied phenomena to take place or, at least, to avoid any human or equipment loss.

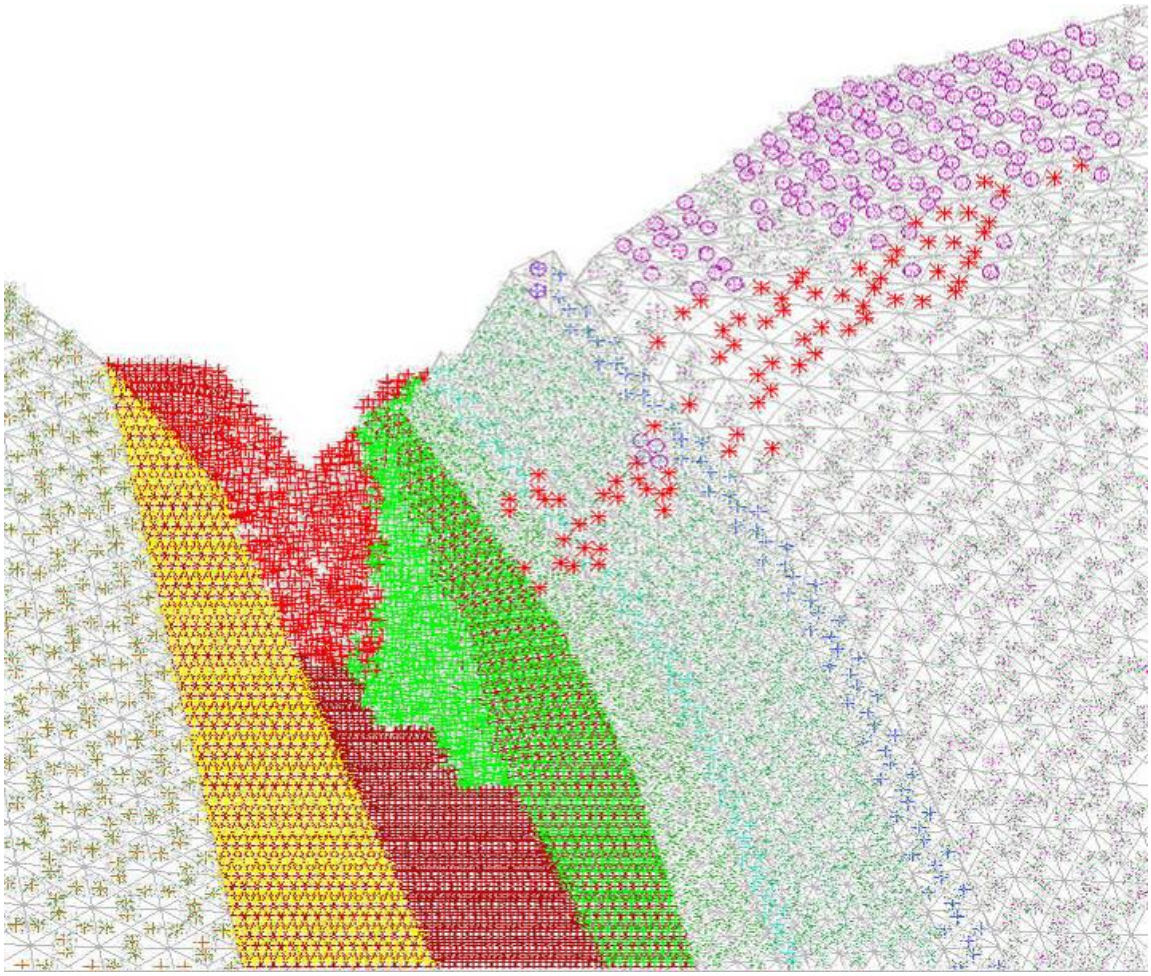

Figure 4. Phase 4 – Plastic deformations (red asterisks) produced by shear stresses

Figure 5. Subsidence in the bottom of Tinyag mine

Figura 6. Tensile crack in a slope of the Tinyag mine

REFERENCES

[i] ITASCA CONSULTING GROUP, 2004. UDEC. Universal Distinct Element Code. Version 4.0. Minneapolis. Minnesotta. USA.

[ii] KVAPIL, R., 1992. 'Sublevel caving'. In: SME Min. Eng. Handbook Littleton, CO: Soc Min Metal Explor; p. 1789–814.

ON THE ROLE AND INFLUENCE OF INTERFACES IN UNDERGROUND DISPOSALS FOR NUCLEAR WASTE

A.C. Dieudonne[*,†], E. Romero[‡], J.P. Radu[*], S. Levasseur[*], R. Charlier[*]

[*] ArGEnCo Department
University of Liege (ULg)
Chemin des Chevreuils 1, 4000 Liege, Belgium
e-mail: ac.dieudonne@ulg.ac.be

[†] F.R.I.A., Fonds de la Recherche Scientifique – FNRS
Rue d'Egmont 5, 1000 Brussels, Belgium

[‡] Department of Geotechnical Engineering and Geosciences
Technical University of Catalonia (UPC)
Campus Norte UPC, 08034 Barcelona, Spain

Key words: Interface finite element, THM behaviour, Nuclear waste disposal

Abstract. *Approaches to model the behaviour of underground disposals for nuclear waste have traditionally assumed perfect contacts between the different materials. However interfaces between the materials may affect significantly the hydration process of the bentonite buffer and later act as preferential pathways for the migration of radionuclides. The paper presents an approach to model interfaces using contact finite elements. The influence of interfaces on the hydration kinetics of a bentonite buffer is highlighted.*

1 INTRODUCTION

In recent years, particular attention has been paid to the behaviour of bentonite-based materials in relation to their use as engineered barriers in deep geological repositories for nuclear waste. In this context, the engineered barrier aims at creating a zone of low permeability that is able to delay the water flow from the host rock, hence the release of radionuclides into the environment.

Depending on the country, different concepts of disposal, with different bentonite-based materials, have been envisaged. In most cases, the materials are either pure bentonite or mixtures of bentonite with sand or excavation products. The sealing material may also take different forms, namely compacted blocks or mixture of powder and pellets.

In all concepts of disposal, the engineered barrier will be initially unsaturated and will be subjected to hydration from the surrounding saturated host rock. During this process, it will tend to expand and will develop swelling stresses. Although transient, this stage is very important as it is believed to directly impact the final state and effectiveness of the system. A good understanding of the hydration mechanisms is thus essential to assess the performance of the engineered barriers and the time needed for their full saturation.

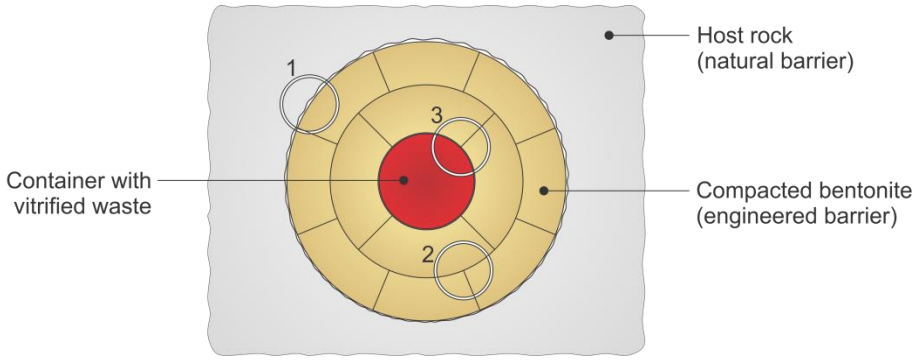

Figure 1: Typical scheme of a deep geological repository for nuclear waste disposal. Interfaces between the different materials are highlighted by the circles 1 to 3.

Traditional approaches for modelling such problems have assumed perfect contacts between the different materials. This strong hypothesis assumes continuity of both mechanical displacements and pore pressures between the materials, which is certainly not true, at least during the first years of the disposal life. Therefore the behaviour of interfaces should be considered for at least two reasons: (1) interfaces significantly affect the transient saturation process of the buffer and (2) they may act as preferential pathways for the migration of radionuclides.

2 FORMULATION OF THE INTERFACE ELEMENT FAIF2

The interface element FAIF2 (Figure 2) is an isoparametric element for two-dimensional analysis. It is implemented in the finite element code Lagamine which has been developed at the University of Liege.

In order to describe the flow not only through the interface, but also within the interface, a three-node formulation is adopted. The finite element FAIF2 uses 2 or 3 nodes on each side of the interface (structure and foundation), as well as 2 or 3 additional nodes inside the interface (interior). The nodes of the structure and the foundation are characterized by 5 degrees of freedom (2 mechanical displacements, water pressure, gas pressure and temperature), while the ones of the interior have only 3 degrees of freedom (water pressure, gas pressure and temperature) and have the same coordinates as the nodes on the structure side of the element (Figure 2).

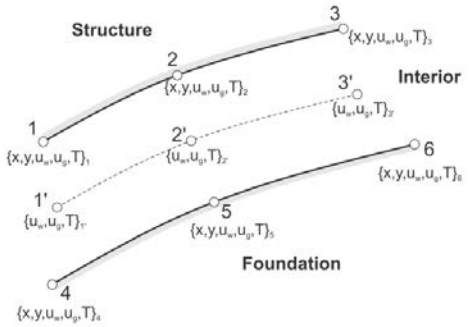

Figure 2: Description of the 2D interface element FAIF2

Different mechanical laws and a multiphase flow law are available to fully describe the THM behaviour of the interface[i,ii].

3 INFLUENCE OF INTERFACES ON THE HYDRATION KINETICS OF BENTONITE PLUGS

The influence of interfaces on the hydration kinetics of bentonite plugs is highlighted through a one-dimensional academic example. Let us consider the contact between two blocks of compacted bentonite (Figure 3). Only block of bentonite is subjected to direct hydration; the second block will progressively saturate in contact with the first block. The contact between both blocks is modelled using the interface element FAIF2. As a first approach, a purely hydraulic modelling of the problem is performed.

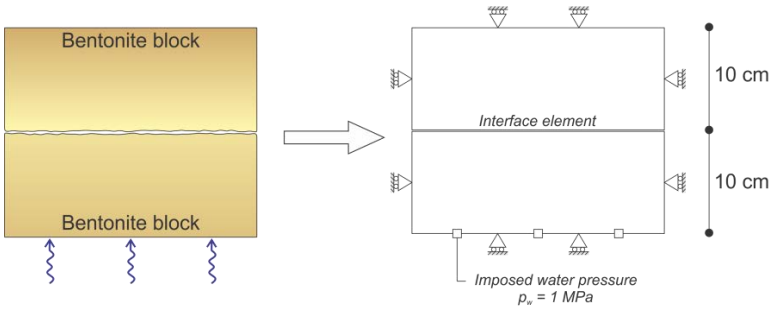

Figure 3: Contact between two blocks of compacted bentonite

In order to describe the transversal flow behaviour of the interface, the concept of transmissivity is used. The transmissivity plays the same role as the permeability is a classical

multi-dimensional analysis and relates the transversal flow rate through the interface to the pore pressure gradient in this same direction.

Figure 4 presents the hydrations kinetics of the bentonite blocks in terms of injected volume of water. For sake of comparison, the problem assuming perfect contact between both blocks of bentonite is analysed as well. During the first year of hydration, the hydration kinetics is not influenced by the interface. Indeed it is controlled mainly by the block submitted to direct hydration. Afterwards, the hydration kinetics is not only controlled by the hydraulic state and properties of the material, but also by the one of the interface. Figure 4 shows that this interface can significantly delay the hydration process, which is a key issue in the framework of nuclear waste disposal.

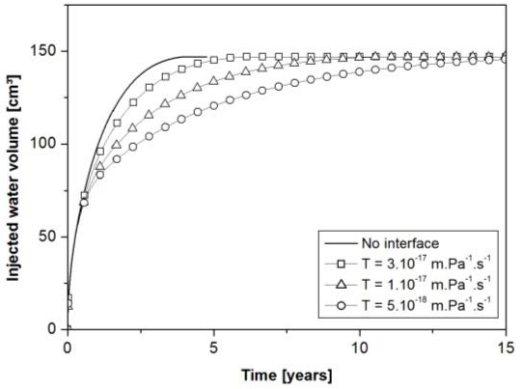

Figure 4: Influence of the interface transmissivity on the hydration kinetics of the bentonite buffer

4 CONCLUSIONS

Interfaces between the different materials of a repository play a critical role regarding the hydration kinetics of the bentonite buffer and the migration of radionuclides. While up to now, most attention has been paid to the THM behaviour of the different materials, the behaviour of interfaces should also be investigated. This characterization requires the development of dedicated laboratory tests, as well as special numerical tools.

ACKNOWLEDGEMENTS

The authors acknowledge the Fédération Wallonie-Bruxelles and the University of Liege for their financial support during the stay of the first Author at the Technical University of Catalonia.

REFERENCES

[i] Guiducci C., A. Pellegrino, J.P. Radu, F. Collin, R. Charlier, 2002. Numerical modeling of hydro-mechanical fracture behavior. In Numerical Models in Geomechanics – NUMOG VIII, Pande & Pietruszczak (Eds.) Swets & Zeitlinger, 293-299.

[ii] Charlier R., F. Collin, P. Gerard, J.P. Radu, 2009. Développement d'un modèle (element fini et loi de comportement) de fracture couple mécanique – écoulement en saturation partielle. Technical report, University of Liege, 47 p.